SDC-91-166

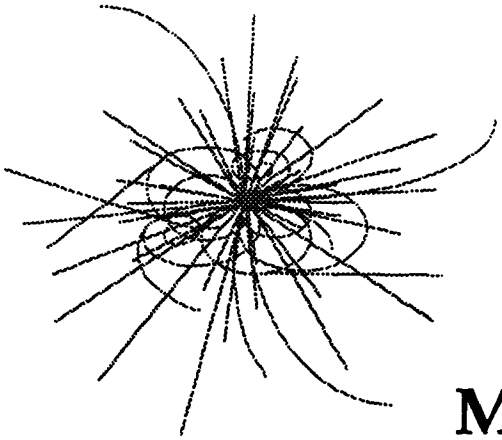

Monthly Report of the Solenoidal Detector Collaboration

November 1991

CONTENTS

Report Summary 1

A. Technical Progress 3

2. University of Wisconsin -- Muon System 3

Muon System 3

Muon Chamber Prototype 3

Preliminary Design (Iron and Coils) 3

3. University of Wisconsin -- Trigger System 11

Calorimeter Level 1 Trigger 11

Trigger System Engineering 12

Trigger Clock/Control 12

4. Fermilab (FNAL) 14

Solenoid Design 14

Magnet working group meeting 14

Technical Proposal 14

Cryogenics 14

Cold Mass Supports 14

Magnetostatic and Other Calculations 15

Calorimetry Engineering 15

Continued Design on Iron Hadron Calorimeter 15

Refinement of Cost Estimates 16

Definition of End Cap Structure Options....16

Test Beam Prototype Construction....16

Data Acquisition System....16

Muon Support and Alignment....16

Calorimeter, FADC....17

5. Argonne National Laboratory (ANL)....18

Lead Scintillator Plate Calorimeter....18

Barrel Calorimeter....18

Barrel Calorimeter Analysis....18

End Cap Calorimeter....18

Lead Creep Tests....18

Fermilab Test Beam....18

Westinghouse Science and Technology Center Subcontract....18

Barrel Design....18

Endcap Design....19

Summary of Parametric Cost Studies Performed Thus Far....19

Bicron Corporation Subcontract....19

8. Los Alamos National Laboratory (LANL)....31

Cost and Schedule Activities....31

Structural Analysis Studies....31

Radiation Length Studies....31

Materials Science Studies....31

Alignment Studies....33

9. ICF – Kaiser Engineers (KE)....34

10. Lawrence Berkely Laboratory (LBL)....35

Computing Systems.....35

16. Martin Marietta.....37

Muon System Costing and Scheduling Phase II.....37

Engineering Services.....38

B. Program Costs.....40

MONTHLY REPORT

OF THE

SOLENOIDAL DETECTOR COLLABORATION

NOVEMBER 1991

REPORT SUMMARY

- **PHYSICAL SCIENCES LABORATORY (PSL) - MUON**

  Additional calculations and texts were undertaken to optimize the muon barrel chamber support system. The 32 cell (9.5m) prototype unit was wired. A 16 cell (1m) unit was gas sealed and readied for testing. Design optimization of the barrel torroid is continuing.

- **PHYSICAL SCIENCES LABORATORY (PSL) - TRIGGER**

  Studies of the calorimeter Level 1 jet Trigger were completed; electronic components are being tested. A revised cost analysis of the overall SDC Trigger was accomplished. Studies began for the new design of the clock and control system distributions and generation.

- **FERMI NATIONAL LABORATORY (FNAL)**

  Calorimetry engineering efforts focused on the iron/hadron systems. Cost estimates were refined and end-cap structure options were explored. ANSYS analyses of various truss configurations for the muon support system were made. Preparations began for establishing the Solenoid design for the Technical Proposal. Efforts continued on the design of associated cryogenic systems.

- **ARGONNE NATIONAL LABORATORY (ANL)**

  The routing of fibers for the barrel calorimeter was explored. The 3-D model of the end-cap calorimeter is undergoing a detailed analysis. Two test modules have been instrumental and installed in the FNAL test beam.

- **LOS ALAMOS NATIONAL LABORATORY (LANL)**

  Design work is continuing on the silicon tracking system. Finite element calculations are in progress to evaluate asymmetric loads on the silicon shells. Properties of the materials in the structure as well as alignment requirements are being investigated.

- **ICF KAISER ENGINEERS (KE)**

  Efforts centered on the construction and support of the forward muon torroids. Support systems were developed to assist in assembly and disassembly operations.

- **MARTIN MARIETTA**

  Detailed cost and scheduling information was developed for the muon system. Revised plans were provided for manufacturing, assembly and installation programs as well as alignment requirements.

A. TECHNICAL PROGRESS

2. UNIVERSITY OF WISCONSIN PHYSICAL SCIENCES LABORATORY (PSL) - MUON SYSTEM

Muon System

Additional calculations and tests were performed to investigate the behavior of barrel chamber monoliths in every octant and arrive at optimal support locations. The feasibility of an internal gas manifold endplate is still under investigation. A supplier has been contacted and early indications are promising. Two versions of this endplate are under study: one that is straight and is for phi chambers because they will have square ends; the other is stepped and is for theta chambers to reduce dead space.

Muon Chamber Prototype

During this month all the cells for the 32-cell 9.5 m prototype were wired. The cell assembly time and cell wiring time were measured and will be incorporated into the cost estimate. All 9.5 meter extrusions received from the extruder were measured for length and squareness tolerance. 6 endplates (2 for 32 cell and 4 for 16 cell prototypes) with wire mounting, screw and gas holes were machined and then measured. Temperature of the plates during machining and measuring was monitored. Effects of various machining operations on plate temperature were observed. The standard deviation for wire mounting hole locations was measured at 6 mocron. Machining time for every hole was measured and will be incorporated into the cost estimate.

One 16-cell 1 m prototype was gas sealed and is ready for tests. The electronics for this chamber are being assembled.

Preliminary Design (Iron and Coils)

The inner radius (IP to flat) for the MBT has been fixed at 6750 mm and the length is fixed at 28032 mm for the technical proposal. The dimensions of the blocks has also changed so their weight stays at 85 metric tones with the new dimensions. The number of blocks decreased from 224 to 192 (16%). Investigation of Z connection requirements and options continues. Information on steel specification and fabrication requirements were gathered and sent to a representative from Brazil. Along the same line, planning for the upcoming trip by delegates from the Soviet Union is underway. Finite element analysis of the MBT is being coordinated with SSCL. This month the modeling concentrated on understanding and improving the model accuracy and boundary conditions rather than actually running cases. Finite element analysis of the support is being coordinated with FNAL. After the first run, the design was modified to balance jack loads, and improve torsional stiffness. The second run showed these changes cut the deflections in half and reduced all stresses to acceptable levels. PSL is also participating in an effort to identify the requirements for safety approval of the MBT.

The forward coils were the focus of attention for the coil work. Two designs were investigated. Both designs use a miter joint in the corner. The feasibility of the type joint is under investigation. One of the designs is a "standard" single helix. The advantage of this is simplicity, bu the disadvantage is a poor thermal profile with one high temp side and one low temp side. The second design uses a double helix with two electrical paths and two water paths. The current would flow in the same direction through each path, but the water would

have a counter flow arrangement to provide local temperature averaging. Pittings and hose for the barrel coil water system were selected. Use of a 45 degree hose fitting allows all the local water connections to be made in the shadow of the coil. A detailed list of tasks, quantities, and tools was prepared for use on a more detailed barrel coil cost estimate.

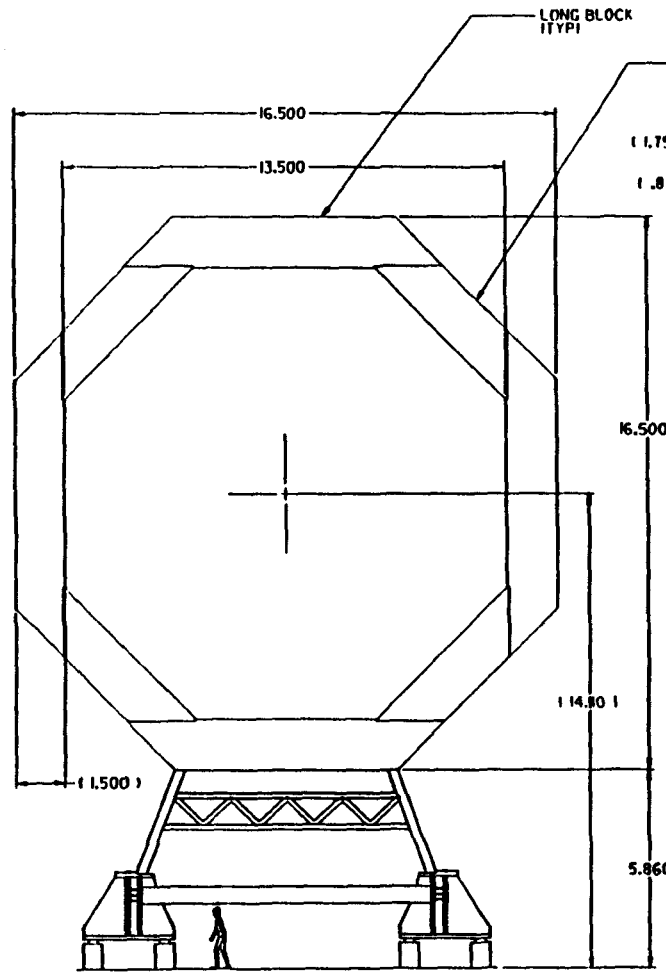

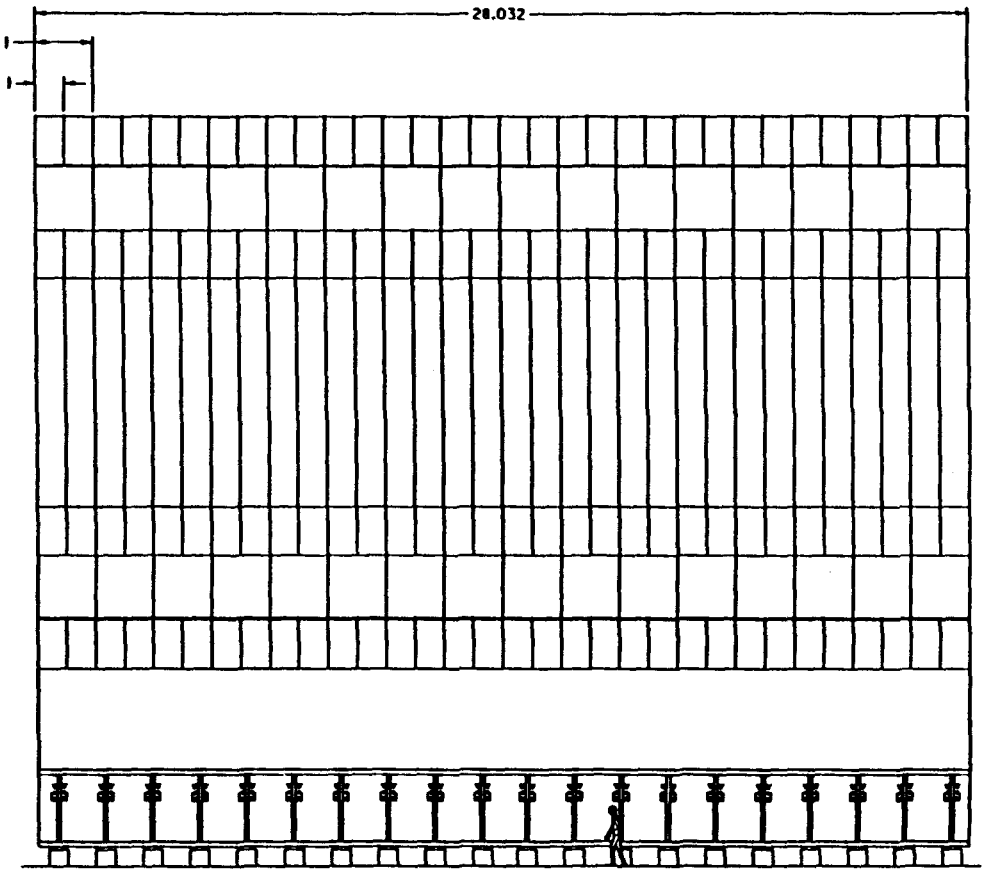

REVISIONS				
ZONE	REV	DESCRIPTION	DATE	APPROVED

QTY	QTY	QTY	PART NUMBER	DESCRIPTION	CAGECO	ZONE	ITEM

LIST OF MATERIALS / PARTS LIST

REF ONLY-NOT TO BE MAINTAINED		
DASH NO.	NEXT ASSY.	USED ON
APPLICATION		

UNLESS OTHERWISE SPECIFIED DIMENSIONS ARE IN MILLIMETERS

TOLERANCE OF SINGLE NUMBERS ±0.5

TOLERANCE OF DECIMALS

.X ±0.5 | .XX ±0.13 | ∠ ±0.5°

1. BREAK ALL SHARP EDGES 0.5 MAX.
2. DO NOT SCALE THIS DRAWING.
3. DIM. TO APPR TOLS - 1982.
4. MAIN. ALL MACH. SURFACES.

DRAWN	LAURA COMBS	DATE 8-21-9
CHKD		
APPD		
APPD		
APPD		
APPD		
APPD		
APPD		
CONTRACT NO.	DE-AC02-89ER40486	

SSC

SDC MBT
PRELIMINARY DESIGN
ASSEMBLY

SIZE	CAGECO	DRAWING NO	REV
C		SDD000084	

SCALE	1:100	WEIGHT	WBS	SHEET 1 OF 1

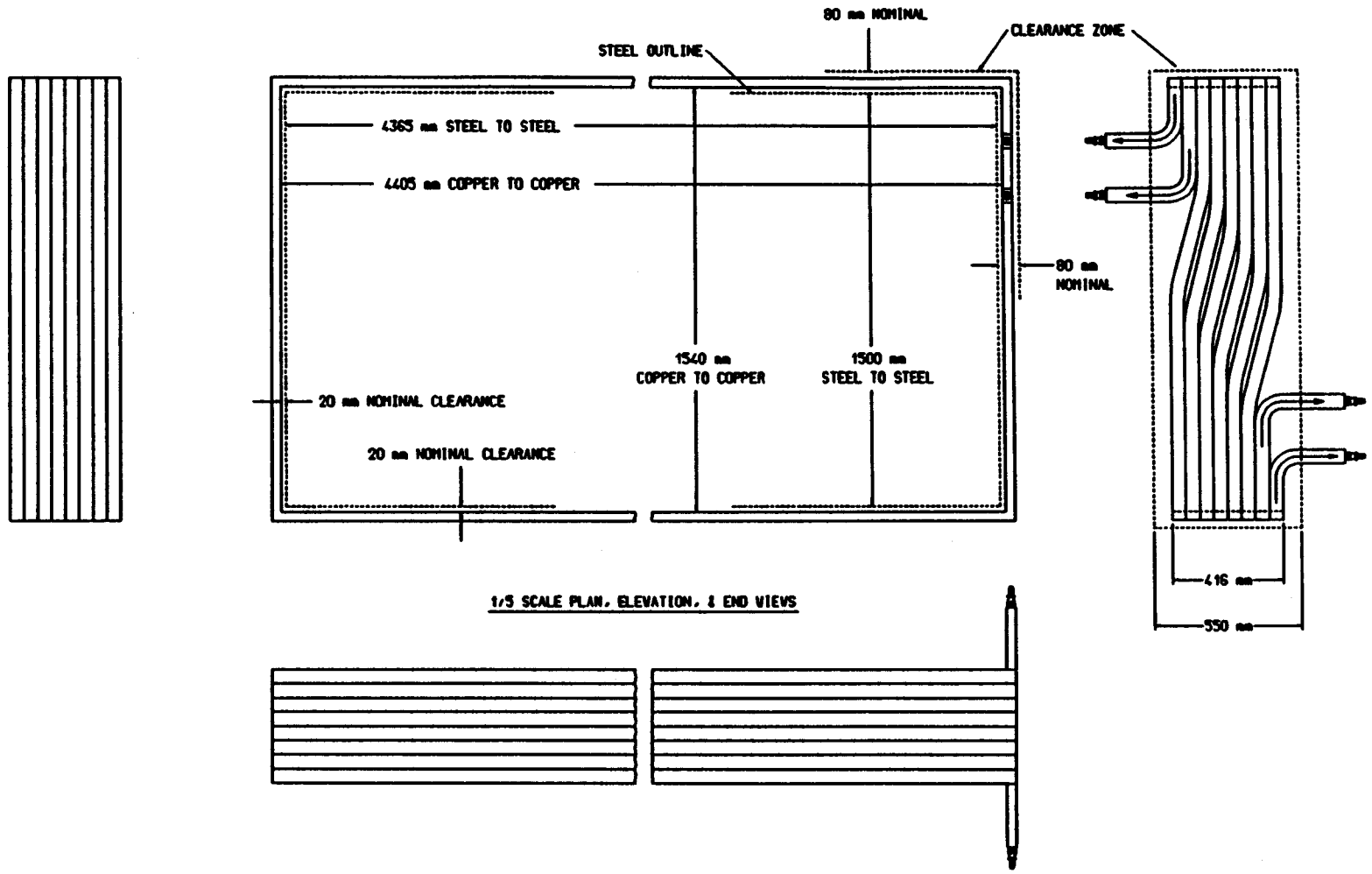

1/5 SCALE PLAN, ELEVATION, & END VIEWS

UNIV. OF WISCONSIN
PHYSICAL SCIENCES LAB
(608) 873-6651
SCALE IS NOTED

PRODUCED BY JJC DRAWING FILENAME COILFORWARD
ON 11/21/91 AT 12:10 PLOTTED AT SCALE 1/1

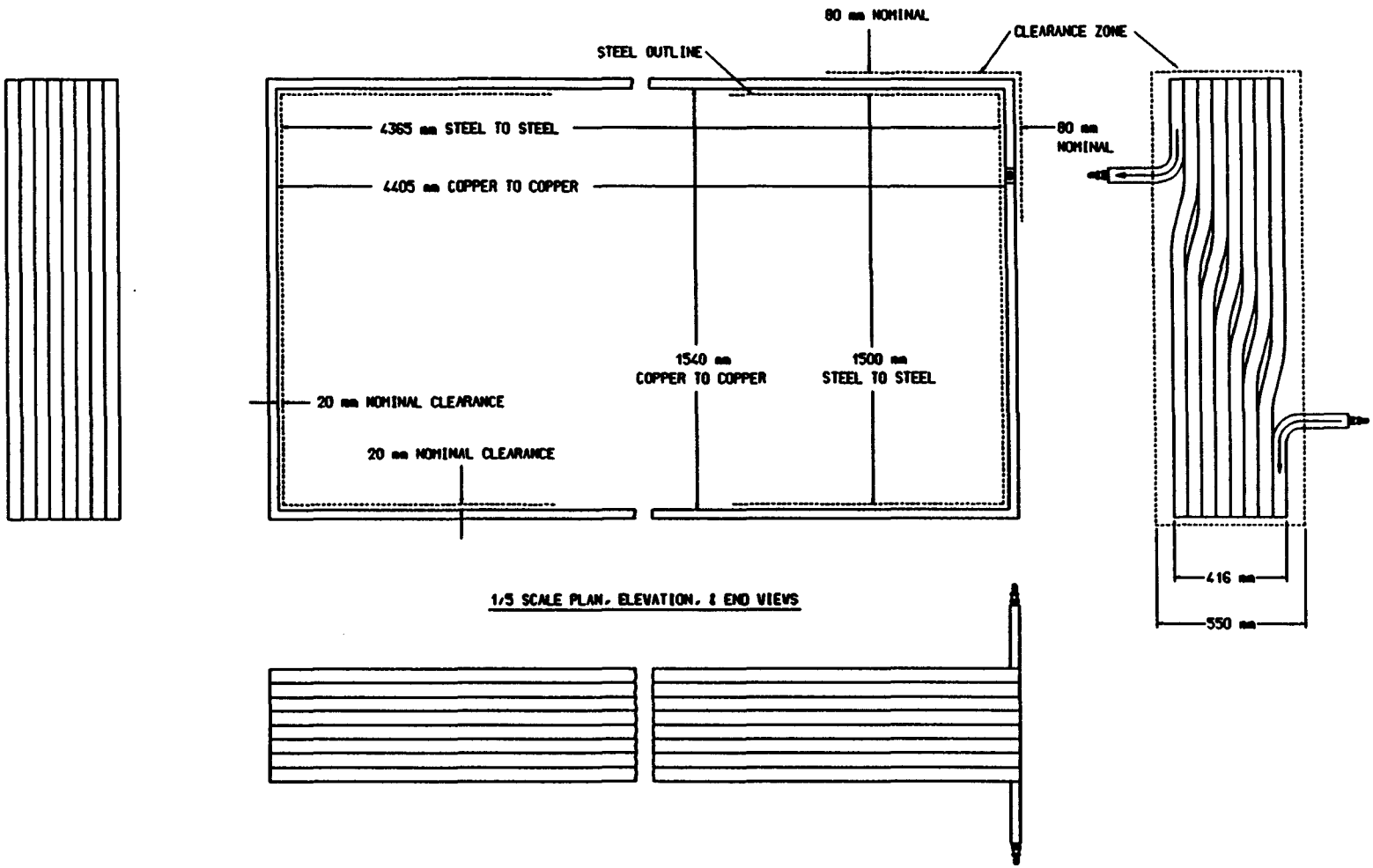

1/5 SCALE PLAN, ELEVATION, & END VIEWS

UNIV. OF WISCONSIN
PHYSICAL SCIENCES LAB
(608) 873-6651
SCALE IS NOTED

PRODUCED BY JJC DRAWING FILENAME COILFORWARD
ON 11/10/91 AT 19:03 PLOTTED AT SCALE 1/1

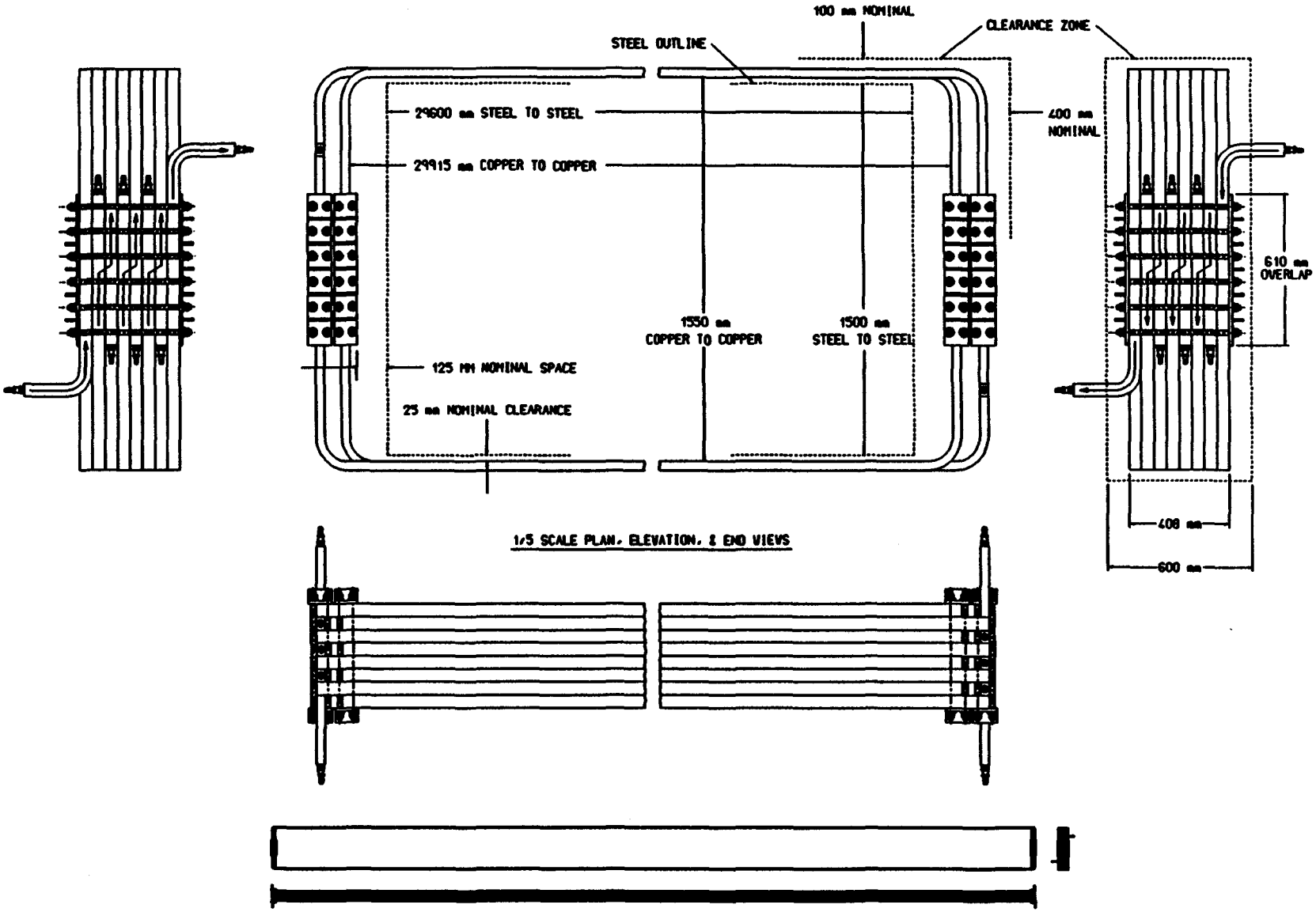

UNIV. OF WISCONSIN
PHYSICAL SCIENCES LAB
(608) 873-6631
SCALE IS NOTED

PRODUCED BY JJC
1/08/91 AT 14:19

DRAWING FILENAME COILFIX
PLOTTED AT SCALE 1/1

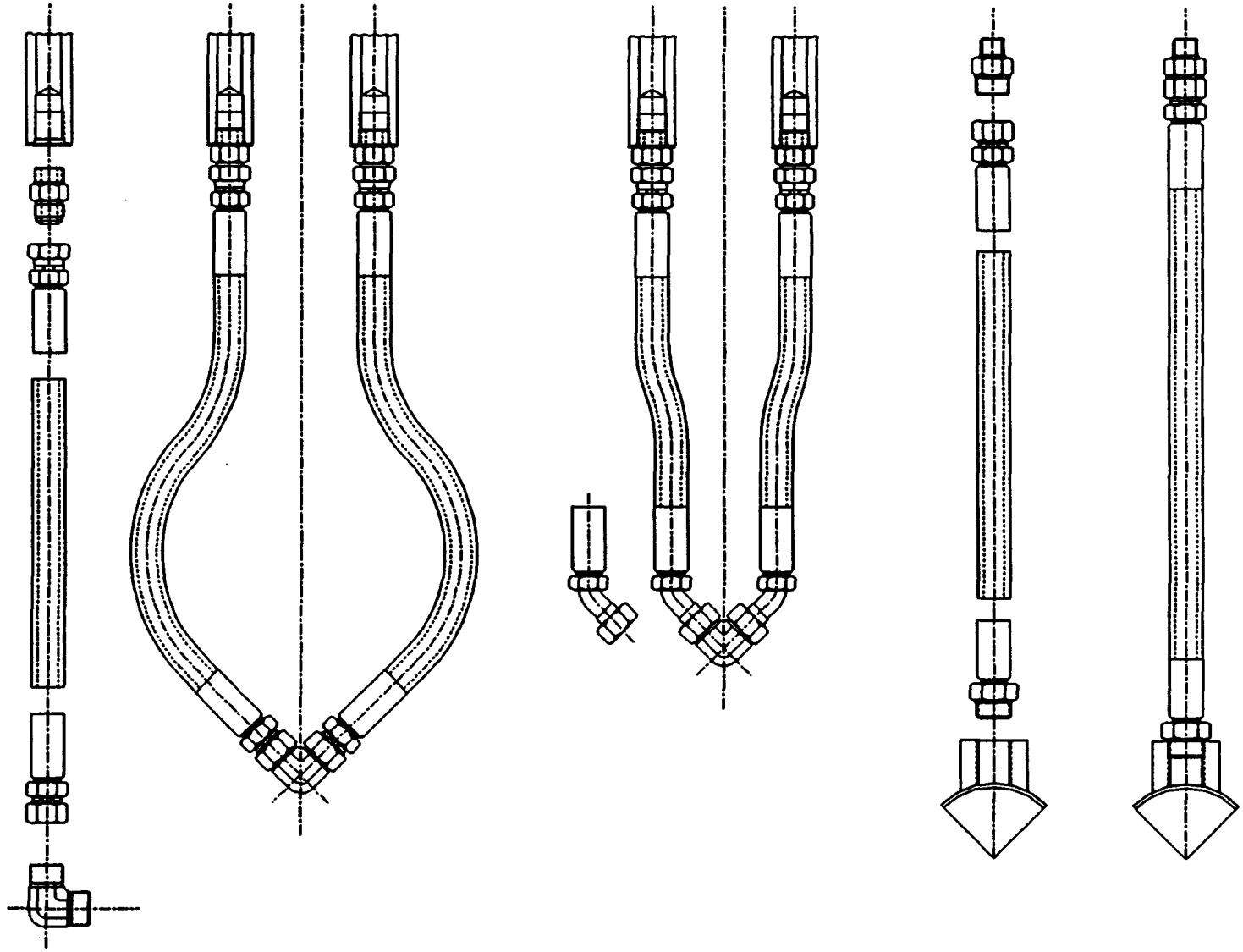

UW PHYSICAL SCIENCES LAB
SSC - SDC HOSE ASSEMBLIES
FULL SCALE

PRODUCED BY GP_JDP DRAWING FILENAME SDCHOSEASSY
ON 11/27/91 AT 16:45 PLOTTED AT SCALE 1/1

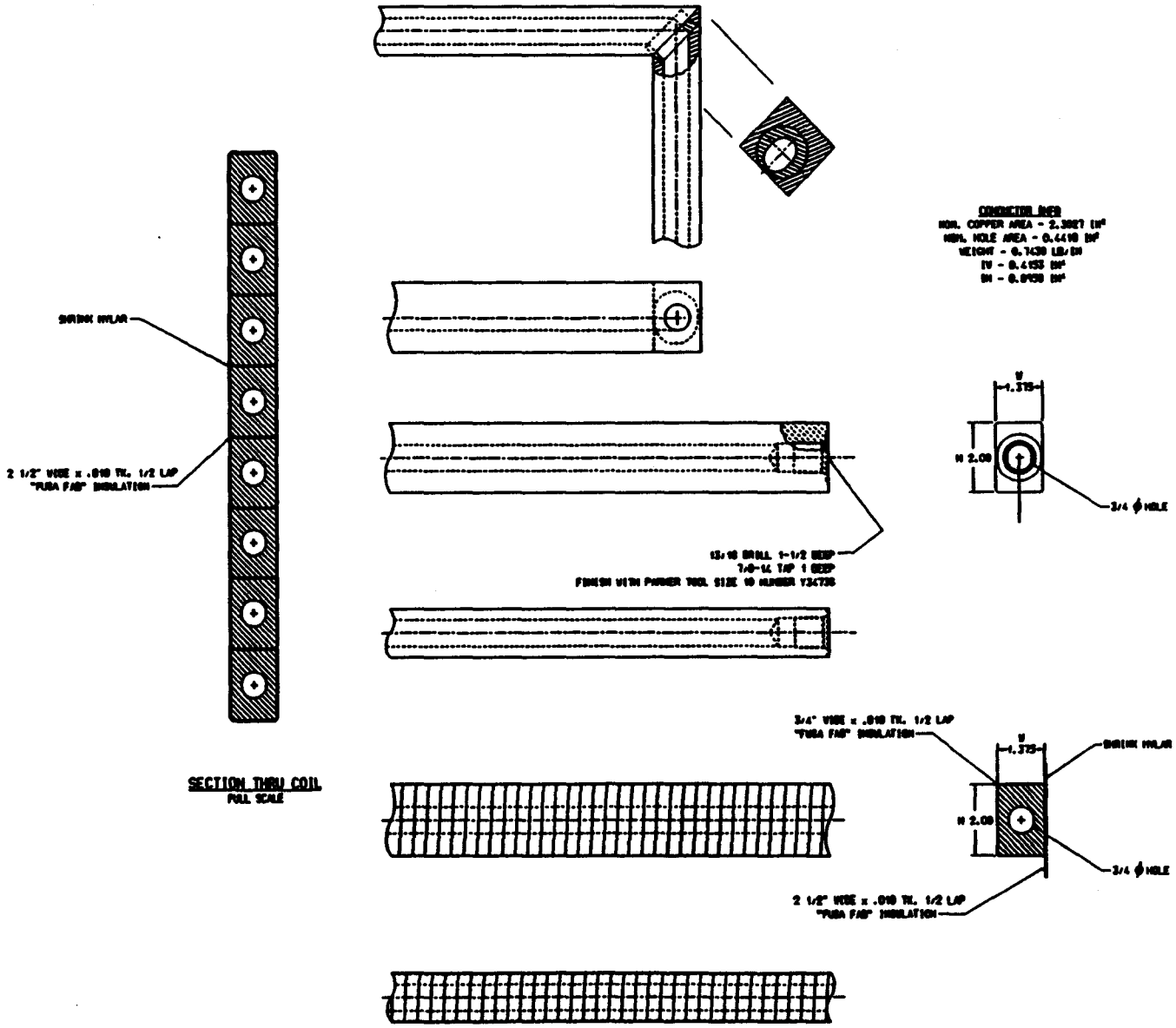

UNIV. OF WISCONSIN
PHYSICAL SCIENCES LAB
(608) 873-6631
SCALE: FULL

PRODUCED BY JJC DRAWING FILENAME COILFORWARD
1/10/91 AT 19:04 PLOTTED AT SCALE 1/1

3. UNIVERSITY OF WISCONSIN PHYSICAL SCIENCES LABORATORY (PSL) - TRIGGER SYSTEMS

Calorimeter Level 1 Trigger

We have performed a study of the design for a calorimeter level 1 jet trigger[1]. Photomultiplier Tube (PMT) currents for the EMC and HAC sections of each trigger tower are fed through a preamp and digitized in a FADC to produce a value for the current. We have designed and tested such a preamp[2] and are testing the first of 20 production surface-mount technology printed circuit boards that are being manufactured for test with the LBL SCA device.

The jet trigger is based on calorimeter information[3]. The basic unit of calorimeter level 1 trigger information is the trigger tower. This is the sum of either the energy in the calorimeter electromagnetic (EM) or hadronic (HAC) compartment in a $.1\eta$ x $.1\phi$ reglon. Generally, this is composed of the transverse sum of 4.05 x .05 EM towers or the longitudinal sum of two .1 x .1 HAC towers digitized on an 8-bit logarithmic scale. This information is sent by the calorimeter isolation/summation crates[4]. The information is received by the calorimeter isolation/summation crates[5]. These sum up the energy in .4 x .4 regions. At this point there is the option to test the energy in the .4 x .4 towers against a series of thresholds, as well as summing up these .4 x .4 sums an array of .8 x .8 sums or two overlapping arrays of .8 x .8 sums. The purpose of the study is to investigate what strategy is best for triggering given the calorimeter information that is available. This includes calculating the effects of the digitization scale and the methods by which towers are combined and tested.

We used 64000 QCD twojet events from 20-400 GeV, and minbias event corresponding to a poisson distribution with mean 1.6 events per crossing were generated as described in Ref. [3]. Jets were looked for in in a calorimeter covering $\eta < 3$. Energy sums were made in each square in two sorts of grids - an overlapping grid, so that the calorimeter was covered twice, and a non-overlapping grid. The sizes of grids used were .2 x .2, .4 x .4, and .8 x .8 squares in η - ϕ. The simulation instead converted the E_t in each trigger tower to an 8-bit logarithmic scale and back to a real number before adding. This implementation is based on [5]. As an alternative, a 9-bit semi-linear scale was used, which consisted of two overlapping 9-bit linear scales with one bit indicating range. For each size of regions searched, both a single array of non-overlaping sums and two overlapping arrays were used.

---

[1]W. Temple, T. Gorski, J. Lackey, W.H. Smith, *SDC Jet Trigger Studies*, U. Wisconsin SDC Note SDC-91-00140, 1991.

[2]D. Panescu, J.. Lackey, P. Robl, W.H. Smith, *An SSC PMT Preamplifier Circuit*, U Wisconsin SDC Note SDC-91-00089, 1991.

[3]T. Gorski, J. Lackey, W.H. Smith, W. Temple, *Isolated Electron Pattern Logoc Design and Performance at the SSC*, U. Wisconsin SDC Note SDC-91-00087, 1991.

[4]W. H. Smith, T. Gorski, J. Lackey, *SDC Trigger Preliminary Conceptual Design*, U. Wisconsin SDC Note SDC-91-00189, 1991.

[5]T. Gorski, J. Lackey, W. H. Smith, *Level 1 Trigger Decision Design for the SDC*, U. Wisconsin SDC Note SDC-91-00088, 1991.

For each of the efficiency levels considered, the largest jet tower size is the most successful, and overlapping towers are more successful than non-overlapping towers. The best results are found by use of a trigger design with overlapping grids of .8 x .9 towers for the primary jet trigger and a prescaled trigger on a non-overlapping .4 x .4 grid of towers at a much lower threshold. We also conclude that the 8-bit logarithmic scale shows better performance relative to range than does the 9-bit semi-linear scale of two 8-bit linear ranges.

Trigger System Engineering

We have continued development of the preliminary conceptual design of the SDC trigger system[4]. A revised cost analysis of the SDC trigger system based on the design has been produced[6]. This includes an analysis of base cost and contingency.

The SDC trigger system cost is based on a particular implementation of the SDC trigger group conceptual design report[7]. The design is described in [4] and has several subsystems. These include the Level 1 Decision Logic [5, 3], the Level 2 Decision Logic [4] and the Trigger Clock and Control System[8]. The basic Level 1 Trigger system interfaces to front-end electronics crates on the detector for the calorimeter, shower max, tracking and muon subsystems. These are connected with optical fibers[9] to the counting house on the surface, which contains the level 1 decision processing crates. These include the Calorimeter Isolation/Summation crates, the Track/Shower Max Match crates, the Isolated Electron Match crates, the Energy Sum/Jet Threshold crate, the Muon Trigger Crates, and final Decision crate.

Trigger Clock/Control

Considerable design effort has been expended on the clock and control. We have begun extensive studies of the new design of the clock and control distribution and generation. This new design results in a trigger system that is "partitionable" in a similar manner to the DAQ system. Generally, clock and control distribution parallels the DAQ processor control distribution and is closely linked to it.

Specifically, we have performed a detailed analysis of the timing of the level 1 decision[10]. All of the data for a 16 nsec crossing observed by a subsystem of the SDC detector must be held in buffers while the level 1 trigger calculations are being performed and the level 1 trigger decision is being propagated back to the subsystem. These buffers must be able to

---

[6]W.H. Smith, R. Craven, T. Gorski, J. Lackey, J. LeBeck, *SDC Trigger Cost*, U Wisconsin SDC Note SDC-91-00091, 1991.

[7]A. Lankford *et al.*, *Conceptual Design of the SDC Trigger from the SDC Trigger Group*, SDC Note SDC-91-00098, 1991.

[8]W. H. Smith, T, Gorski, J. Lackey, *SDC Global Level 1 Processor: Clock & Control*, U. Wisconsin SDC Note SDC-91-00090, 1991.

[9]M. Thompson, *Fiber Optic Data Transmission for the SDC Detector*, U. Wisconsin SDC Note SDC-91-00092, 1991

[10]T. Gorski, J. Lackey, W. H. Smith, *SDC Trigger Preliminary Conceptual Design*, U. Wisconsin SDC Note SDC-91-00139, 1991.

store an additional crossing every 16 nsec and keep this even t in storage until the level 1 decision arrives. If the decision is to accept, the data from the selected crossing are stored for future processing. If the decision is to accept, the data are discarded. The time interval between the interaction occurring at the interaction point and the arrival of the level 1 decision signal at the buffer containing the information from that interaction is called the pipeline length. If a subsystem has insufficient pipeline length, this means that it lacks the storage capacity to hold the number of crossings that occur between the time of the interaction and the time of arrival of the level 1 decision. Since the front end electronics are constantly writing crossings into their buffers, if these buffers are too short, the front end electronics will be forced to either write over the crossing before the level 1 decision arrives, or stop writing crossings until the level 1 decision arrives. In either case, data is lost and the system experiences deadtime.

The pipeline length is the sum of the collection time of the data from the interaction, the generation of subsystem information to be used in the trigger calculation (trigger primitives), the propagation of this information to the global level 1 trigger decision logic, the calculation of the level 1 decision (either accept or reject), and the propagation of this decision back to the subsystem. The critical timing path is determined by the subsystem that takes the longest to send it trigger data to the level 1 decision logic and the subsystem that has the shortest readout pipeline buffer.

We have produced a detailed calculation of the level 1 pipeline length by going through each of the contributions above [10]. Each subsystem is examined and its pipeline length is calculated, both its contribution to the level 1 decision time, and the storage time necessary for holding data until the arrival of the level 1 decision. The initial conclusion is that a pipeline length of 4 μsec is adequate.

4. FERMILAB (FNAL)

Solenoid Design

Magnet working group meeting

The SDC solenoid magnet working group met on November 7 and 8. Akira Yamamoto (KEK) and Bob Kephart (FNAL), co-leaders of the working group attended, along with members of the Fermilab team and Bob Richardson from SSCL. The agenda included discussions of the detector magnet, the technical proposal, and the prototype magnet. The meeting notes and copies of the FNAL and KEK viewgraphs are documented in Fermilab SDC Design Notes.

Technical Proposal

The superconducting solenoid chapter of the Technical Proposal will be edited by A. Yamamoto. Four members of the Fermilab team wrote the sections of it for which Fermilab was responsible: magnetostatics, support system alternative, chimney and control dewar, isogrid outer vacuum shell alternative. A. Stefanik and R. Fast met with John Elias, Bob Lavelle, and Georges Leskens of the SDC Safety Analysis Group to begin the preliminary hazard analysis which will appear as part of the Technical Proposal.

Cryogenics

A preliminary flow schematic was made of the control dewar, which is the interface between the solenoid cryostat and the transfer line provided by the SSCL. The effect of reducing the chimney diameter, both for a short length and for its entire length, on the pressure drop and vacuum pumping speed was calculated. Work on the calculation to determine the helium relieving rate and pressure rise during a quench continued.

A. Stefanik participated in a review of the preliminary design and the design requirements for the VLPC cassette and cryostat being developed by Rockwell International.

The work on the isogrid development for the prototype vacuum vessel continued in November. The machining of the first of two isogrid test panels was completed in the Fermilab machine shop, the second should be completed early in December. We plan to brake-form these test panels to the radius of the prototype shell, 2060 mm, but this purchase requisition has been held due to the financial problem. The outer diameter of the outer vacuum shell of the prototype has been increased by 20 mm to provide more space in the vacuum annulus. This led to a redesign of the isogrid panels and slight changes in the node spacing. The working group also decided that the annular bulkheads at the ends of the prototype vessel should be made removable for inspection and possible repairs. The incorporation of O-ring grooves and a bolting flange on the inner shell resulted in additional engineering and design which is not yet complete.

A. Yamamoto showed a 1 square-foot sample of vacuum brazed aluminum honeycomb, which he proposes for the outer vacuum shell of the detector magnet cryostat. He agreed to pursue this alternative with the Japanese company.

Cold Mass Supports

It was decided at the working group meeting that both KEK and Fermilab would consider the separated function type of support system, and that each group would design a system with

the same load capability so that the two systems could be compared. It was agreed that the Composite Wound Delta combined function support required more analytical and test work than was available at this time and that it would not be further considered. It was also agreed that the separated function supports would be attached to the annular bulkhead at their 300-K ends. In this way, the isogrid or honeycomb outer vacuum shell would not carry the weight or de-centering forces.

Magnetostatic and Other Calculations

Several magnetostatic models were created based on realistic calorimeter dimensions to look at the effects of iron endwall location on coil forces. Radial and axial decentering forces were found for five endwall locations. Magnetic field contour plots were made and several field maps generated for use in the GEANT simulations being done at the SSCL.

A 46-mm (1.81-inch) thick honeycomb is proposed by A. Yamamoto for the detector magnet cryostat. The isogrid design being so far considered by Fermilab is 56 mm (2.2 inches) thick. In order to more appropriately compare these alternatives, a preliminary study of a 46-mm isogrid was undertaken. A numerical method was used to solve the simultaneous equations for the collapse pressure, which involve six independent parameters. Good agreement was gotten when the parameters associated with the 56-mm design were used. We estimate that a 46-mm isogrid will have to have a weight effective thickness of 13 mm in order to have a collapse pressure of two atmospheres.

The same computational method is being used to study the effect of the machining tolerances on the collapse pressure and the effective thickness. The goal here is to discover which dimensions need to be tightly toleranced and which can have looser tolerances. Tight tolerances, less than 0.1 mm (0.004 inches), will increase the machining cost of the isogrid panels. It is clear from the preliminary work that the skin thickness must be held to a tolerance of about 0.1 mm; increasing the tolerance to 0.2 mm results in a unacceptably low collapse pressure.

Calorimetry Engineering

Continued Design on Iron Hadron Calorimeter

November saw a number of developments for SDC calorimetry. The decision was finally reached to make the first hadron section in both the barrel and the end cap out of steel. This allowed Fermi and Argonne to come to some agreements in design, however it became clear by the end of the month that we are still a long way away from a concensus design. We have had to reverse a number of decisions taken at the last collaboration meeting in Dallas, because the combination of forcing the barrel to have 28 towers ending at $\eta = 1.4$, and maintaining the current length of the tracking volume produces a very nasty corner between the barrel and end cap around the end of the solenoid. The bracket which supports the solenoid is forced to be projective, making it appear much longer to incident particles, and one EM tower between the barrel and end cap must be sacrificed. This layout was pushed strongly for by Dick Hubbard of the Shower Max group in Saclay because it best satisfies the numerology of the shower maximum detector in the EM section, however it also became clear that most members of the calorimeter group do not understand Hubbard's basic assumptions in his trigger numerology. We are in the process of asking him for a clarification of his insistence that the number of towers in the half barrel be divisible by 4.

The design currently favored at Fermi is to have the barrel end at $\eta = 1.3$ and have 26 towers in the barrel at exactly $\delta\eta = .05$ segmentation. The remaining item to be worked out with

Argonne is the exact structure of the barrel em calorimeter. There are several designs on the table, but it looks like only one will best satisfy the features of the em requirements.

Refinement of Cost Estimates

In November, we also started a new impetus to refine the cost estimate for the steel absorber and look at refining the costing model for the scintillator tiles. We are planning to hold a vendor meeting at Fermi on December 18 to discuss with steel vendors various options on fabricating the calorimeter wedges to arrive at the cheapest design which satisfies all requirements. We hope to get a first pass on the steel delivery schedule form this meeting as well.

One change that we've made in the scintillator cost model is to separate the cost models for regular calorimeter tiles and shower max tiles. There are a large number of shower max tiles in the detector which we coasted as identical to other tiles in the first cost estimate done by Westinghouse, ANL, and Fermi. A new technique for ganging groups of shower max tiles together into larger pieces may allow us to cut the cost estimate of these tiles by a factor of 6 or more.

Definition of End Cap Structure Options

LBL, Argonne, and Fermi all spent a great deal of time this month coming up with different configurations for the end cap calorimeters. We have arrived at a plethora of designs all of which satisfy slightly different sets of assumptions about radiation damage to the tiles and tile replacement scenarios. We will continue to study these designs as more is understood about the activation problems with detector materials and exposure limitations to technicians working on tile refurbishment.

Test Beam Prototype Construction

The steel hadron block was finished being welded and machined this month. Now it has been stuffed with 2 towers of tiles and is being readied for installation in the MP 9 beam line. This block gives us another data point to compare with estimates we are getting on full sized wedges, and has already shown us problems with its construction that we should avoid in the real thing. It should be ready for installation on Monday, 12/9/91.

Data Acquisition System

DAQ Costing & Other Project Management: Time was spent in October on the descoped costs in preparation to when a full detailed descoped cost estimate will be required.

Scintillating Tile Calorimetry, Scintillating Fiber Tracking Test Beam Project: Effort included finishing the artworking of the Tracking and continued tests of the Test Transmitter Module.

Conceptual SDC DAQ Design Document: This document was extensively edited in November. Writing began also on the DAQ part of the technical proposal.

Muon Support and Alignment

ANSYS analyses of various truss configurations were made to make preliminary decisions on member sizes and to evaluate the prospect of supporting the trusses at four locations instead of ten. Made preliminary sketches of compliant bearing assemblies which may be necessary to accommodate deflections of the barrel torroid. A designer has begun making

drawings of the bearing assemblies and kinematic supports. Alignment items are being detailed.

The Technical Design Report on Alignment is being written. Review of Addendum C of the Engineering Note for the 50mm dipole magnets to be used in the string test at the SSC has been completed, and the Note for magnet DCA-312 signed.

The prototype Migatron Ultrasonic distance measuring system has been under long term serial port readout. As observed in the short term reading histograms, we continue to observe 0.25mm FW distributions which still wander in long term over a range of 2.25mm. Temperature corrections seem to work but there are shifts in the readings periodically. Long term tests continue.

Extended stability tests on the Keyence LB11, LB-70 high resolution laser diode distance measuring system in an optically shielded configuration indicate a direct in phase small temperature variation. Fixed distance readings can be corrected to yield a residual fluctuation of +- 5 microns. Without optical shielding, there are some ambient light background fluctuations (in the lab) superposed on the thermal fluctuations.

Tests on alternate new source diodes for the transverse position optical alignment sets have been delayed in order to set up and readout some precision inclinometers. Two sets of thermally stabilized dual transducer units have been established and are now being monitored. All four sensors are aligned along the axis of our test bench. With this redundancy, we should be able to separate physical and systematic fluctuations.

Calorimeter, FADC

The Integrator/Digitizer chip which was fabricated in August did not work and needed to be refabricated. Chips from the second run also did not work. In both cases the foundry incorrectly made the chip masks. The foundry has for the third time made the Integrator/Digitizer chip (with good masks) and preliminary tests indicate that the chip is functioning as expected. Specifically, the current splitter appears to divide the current over a wide range to better than 1% accuracy. Both the high and low current ranges of the current splitter are functional. The response time of the splitter is quite fast. The risetime of the split current is in the range of 2/4 ns which is fast enough for our application. Thus far no fatal problems have been found on the chip. Testing on additional chips will begin to characterize chip performance spread.

The models for the TI BiCMOS process have been obtained and some preliminary SPICE runs have been performed on the splitter chip using those models.

Continued testing of the present current splitter design and investigate transfer of the design to the TI process. The foundry problems which occurred at Orbit have delayed progress by about 10 weeks.

A new design of the fast floating point adder chip has been completed and the chip has been submitted for fabrication. This version is a major redesign of the second clock tic and should provide significantly improved performance over the first version which has been extensively tested. The new design is expected back in 5-6 weeks.

5. ARGONNE NATIONAL LABORATORY (ANL)

Lead Scintillator Plate Calorimeter

Barrel Calorimeter

The early part of November was devoted to exploring potential fiber routing for the barrel calorimeter. This first attempt demonstrates the feasibility of using either single or double fiber readout of the scintillator tiles. Single fiber readout is by far the easiest to accommodate, but double fibers will fit in the designed radial gap of 3mm. The gap must increase at the EM/HAD1 boundary to accommodate an extra layer of fibers. Figures 1 and 2 show the current fiber routing for an ANL Model B calorimeter barrel.

Barrel Calorimeter Analysis

The data acquired from the FEM analysis has been analyzed and the plots shown in Figs. 3 - 7 show the module-to-module loads as a function of the module position in the barrel.

End Cap Calorimeter

Design drafting work on the end cap calorimeters was halted in November and the work that continued related to bringing the FEM analysis of the end cap to a level paralleled to that of the barrel. The 3D model of the end cap has been iterated several times to compensate for fluctuating design parameters, but the model we now have is being analyzed and preliminary data has been obtained. There appear to be no major differences between the Argonne analysis and the ANSYS analysis reported by Westinghouse in the October monthly report. Figures 8 and 9 represent the current FEM 3D models and Fig. 10 is a plot of intermodule loading along the HAD1/EM boundary.

Lead Creep Tests

The long term creep test is continuing at ANL with the creep rate having reached a steady state. The rate of creep is $\approx 8 \times 10^{-5}$ in/in/wk when subjected to a load of 80 lb./in^2.

Fermilab Test Beam

The second test module was instrumented during the month of November. The mounting of the second module into the test beam was accomplished and all of the mounting hardware performed as expected. The two module array was mounted in the test beam on November 27. First beam was shot into them on December 1 and the remainder of the test program is now well underway.

Westinghouse Science and Technology Center Subcontract

Barrel Design

Completions of the work to be carried out under this contract was accomplished within October. This basically comprised an evaluation of the incremental costs of replacing a lead HAC1 section with a steel variant based on the HAC2 design. The final report is in preparation.

Endcap Design

Task 1: *Outer Support Structure:* The preliminary design of the outer support steel has progressed. The design has been modified to allow attachment of the nitrogen purge system, fastening of adjacent wedges, assembly of fibers and PMT's and assembly of the absorber wedge.

Task 2: *HAC2*: An assembly plan for HAC2 wedge, with the HAC1/HAC2 joint, has been developed.

Task 3: *ANL Integration Analysis:* Management efforts have continued at a minimal level to insure progress and proper prioritization of efforts. The SDC meeting was attended on November 12-15, 1991.

Task 4: *Lead vs. Iron and Misc. Costing:* The lead vs. iron cost studies were performed and the results were reported to the calorimeter group.

Summary of Parametric Cost Studies Performed Thus Far

Distinguishing characteristics of the cases considered are given in the attached Table.

- *Case 22: $159.2M.* This case is similar to the "November 14 consensus design". The only change is that the BHAC2 cell size has been increased to 57.15 mm (2.5") to make it exactly twice the BHAC1 cell size. The end cap HAC2 cell size increased to 114.3 mm (4.5") for the same reason.

- *Case 23: $155.7M.* This is Case 22 with a coarser EM. Savings = $3.5M.

- *Case 24: $143.5M.* This is case 23 with HAC1 xverse granularity changed from .05 to .1. Savings = $12.2M.

- *Case 25: $155.9 M.* Case 22 with H1/H2 boundary moved in approximately 1λ. Savings = $3.3M.

- *Case 26: $162.6M.* Case 22 with H1/H2 boundary moved out approximately 1λ. Savings = $3.4M.

Bicron Corporation Subcontract

A program of scintillator development and testing in conjunction with the Fermilab group (Bross and Pla) has been initiated. This includes production of samples of pure polymer in addition to scintillator for testing. Variables to be evaluated include cross linking, molecular weight, free monomer, additives and processing cycle. Free monomer and molecular weight distribution will now be measured at Fermilab using gas chomatography; diffusion measurements will be carried out at Sandia Labs. Work on identifying an efficient red shifter and promising additives and stabilizers is continuing.

Calorimeter Costing
Distinguishing Parameters; 02 December 1991

	Case 22	Case 23	Case 24	Case 25	Case 26
Barrel EM					
PB thk (mm)	3.18	4.0	4.0	3.18	3.18
Cell thk (mm)	9.18	10.0	10.0	9.18	9.18
Absorber layers	36.0	29.0	29.0	36.0	36.0
Depth (λ)	0.97	0.95	0.95	0.97	0.97
Barrel HAC1					
Xverse seg	0.05	0.05	0.1	0.05	0.05
Absorber layers	32.0	32.0	32.0	25.0	39.0
Depth (λ)	4.95	4.95	4.95	3.87	6.03
Barrel HAC2					
Absorber layers	12.0	12.0	12.0	15.0	9.0
Depth (λ)	4.13	4.13	4.13	5.16	3.10
End Cap EM					
Pb thk (mm)	6.35	8.0	8.0	6.35	6.35
Cell thk (mm)	12.35	14.0	14.0	12.35	12.35
Absorber layers	22.0	18.0	18.0	22.0	22.0
Depth (λ)	1.05	1.05	1.05	1.05	1.05
End Cap HAC1					
Xverse seg	0.05	0.05	0.1	0.05	0.05
Absorber layers	21.0	21.0	21.0	17.0	25.0
Depth (λ)	6.43	6.43	6.43	5.20	7.65
End Cap HAC2					
Absorber layers	7.0	7.0	7.0	9.0	5.0
Depth (λ)	4.53	4.53	4.53	5.82	3.23
COST (M$)	**159.2**	**155.7**	**143.5**	**155.9**	**162.6**

Tile/Fiber Model-B Calorimeter

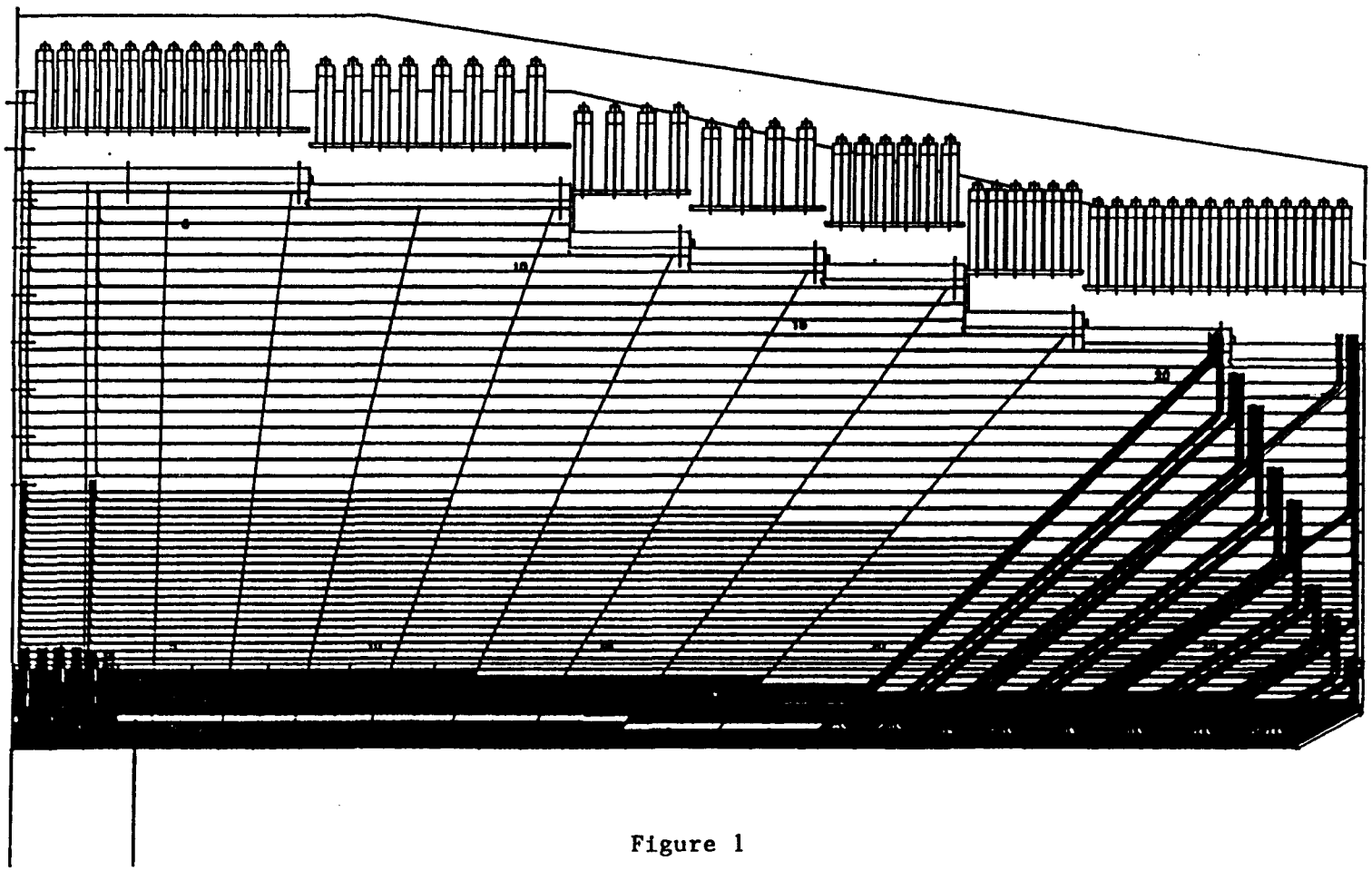

Figure 1

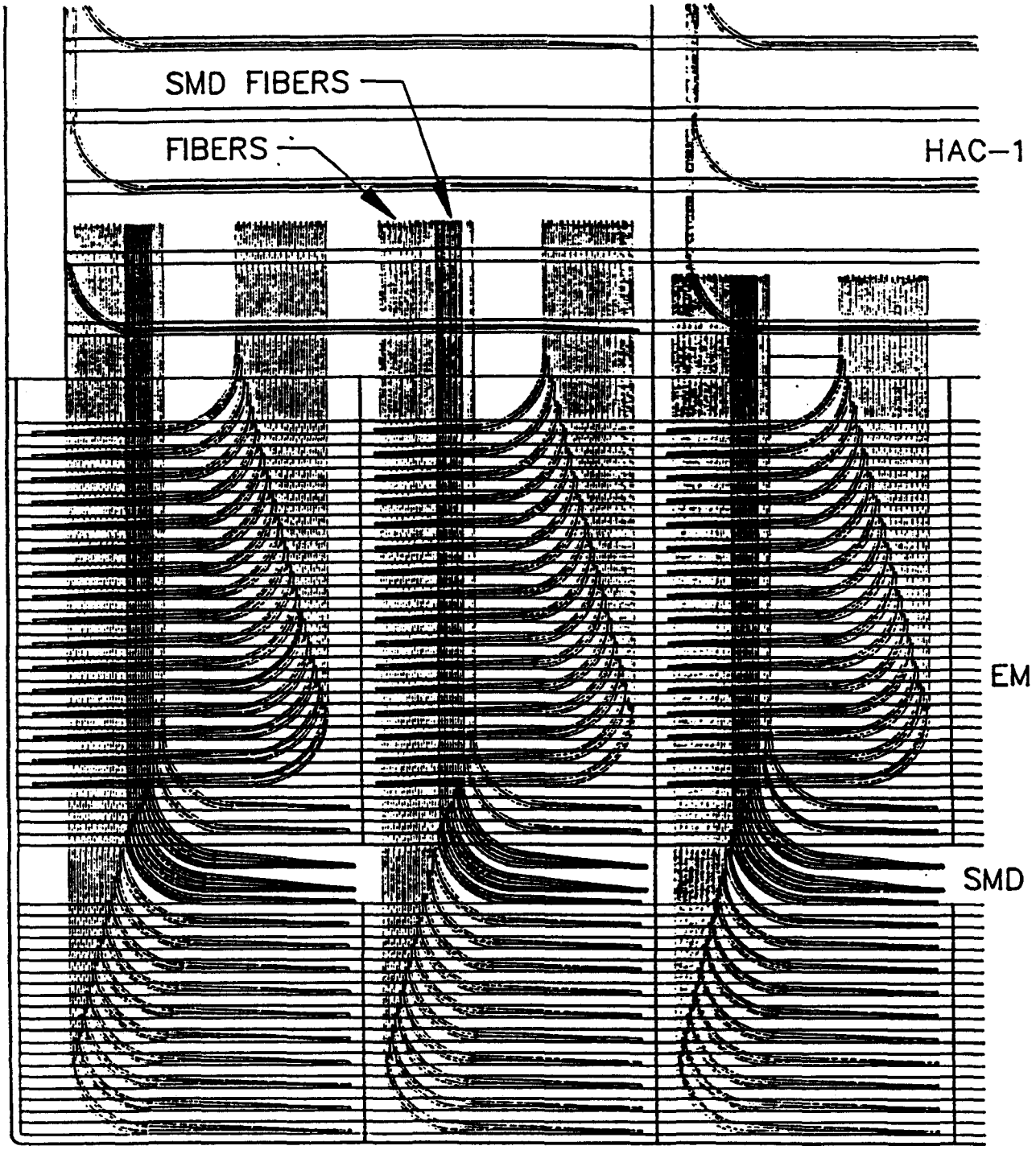

B-CAL Fiber Routing

ARGONNE NATIONAL LABORATORY

Figure 2

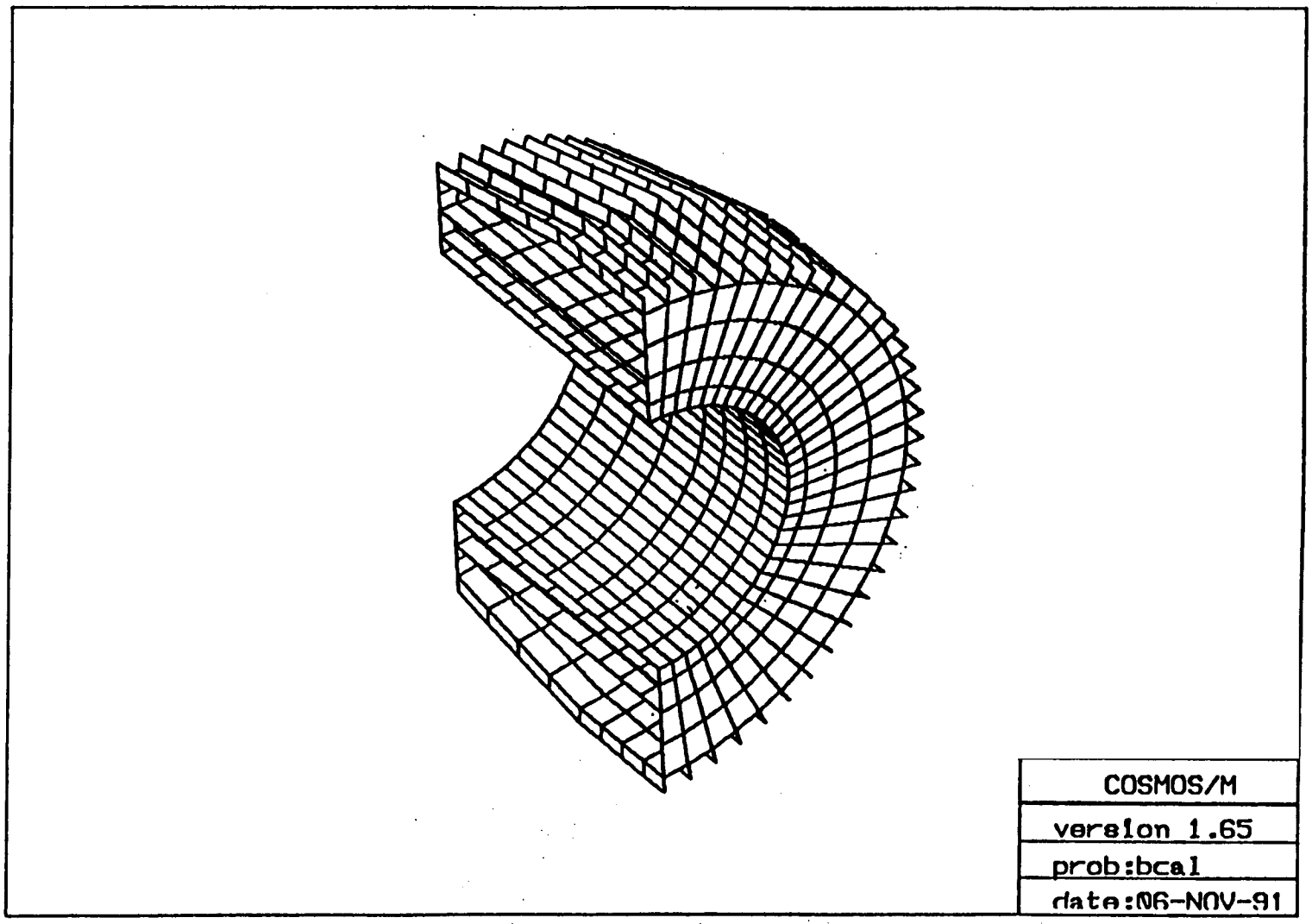

Figure 3

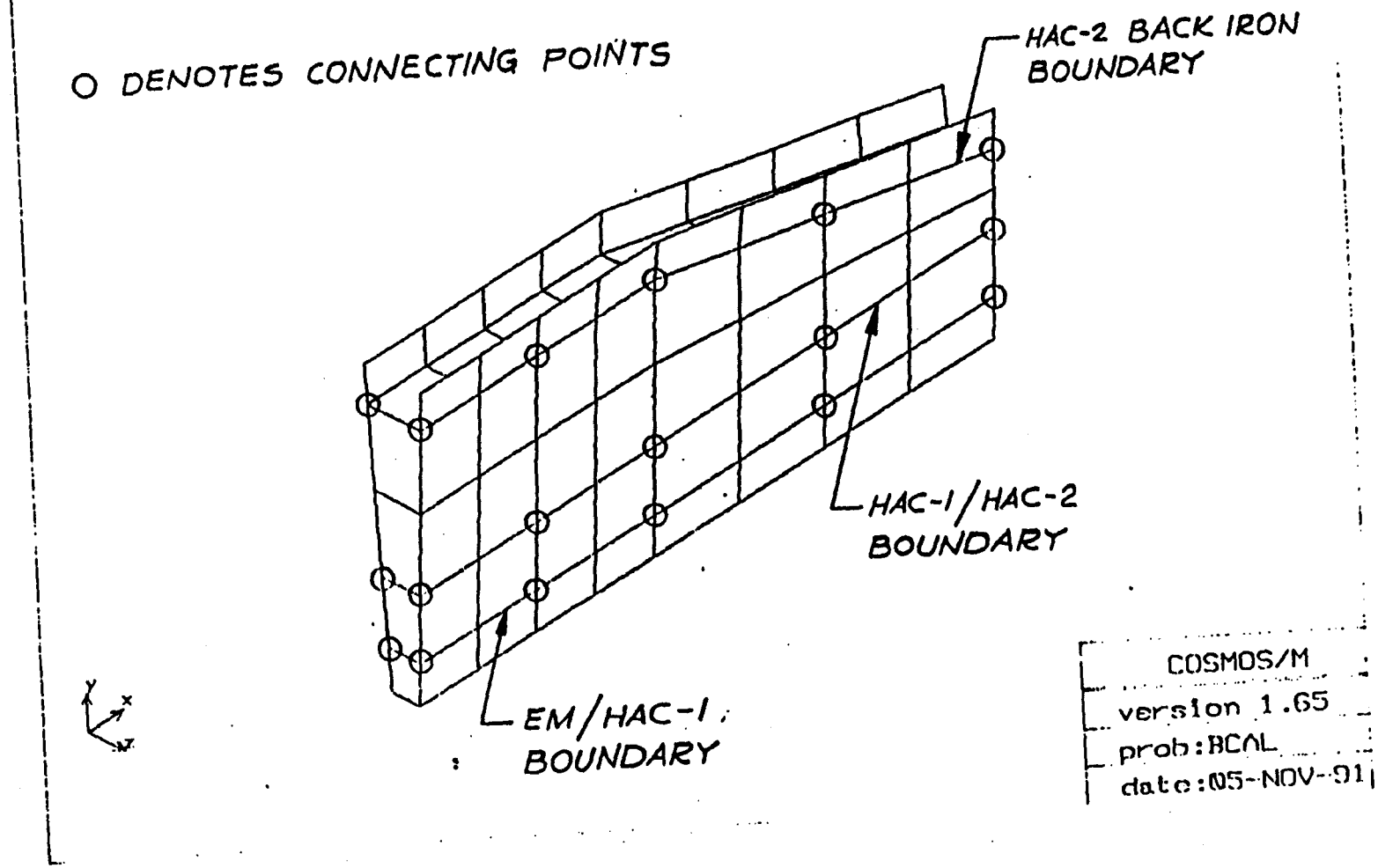
O DENOTES CONNECTING POINTS
HAC-2 BACK IRON BOUNDARY
HAC-1/HAC-2 BOUNDARY
EM/HAC-1 BOUNDARY
COSMOS/M
version 1.65
prob:BCAL
date:05-NOV-91

Figure 4

FORCE ALONG THE BACK IRON

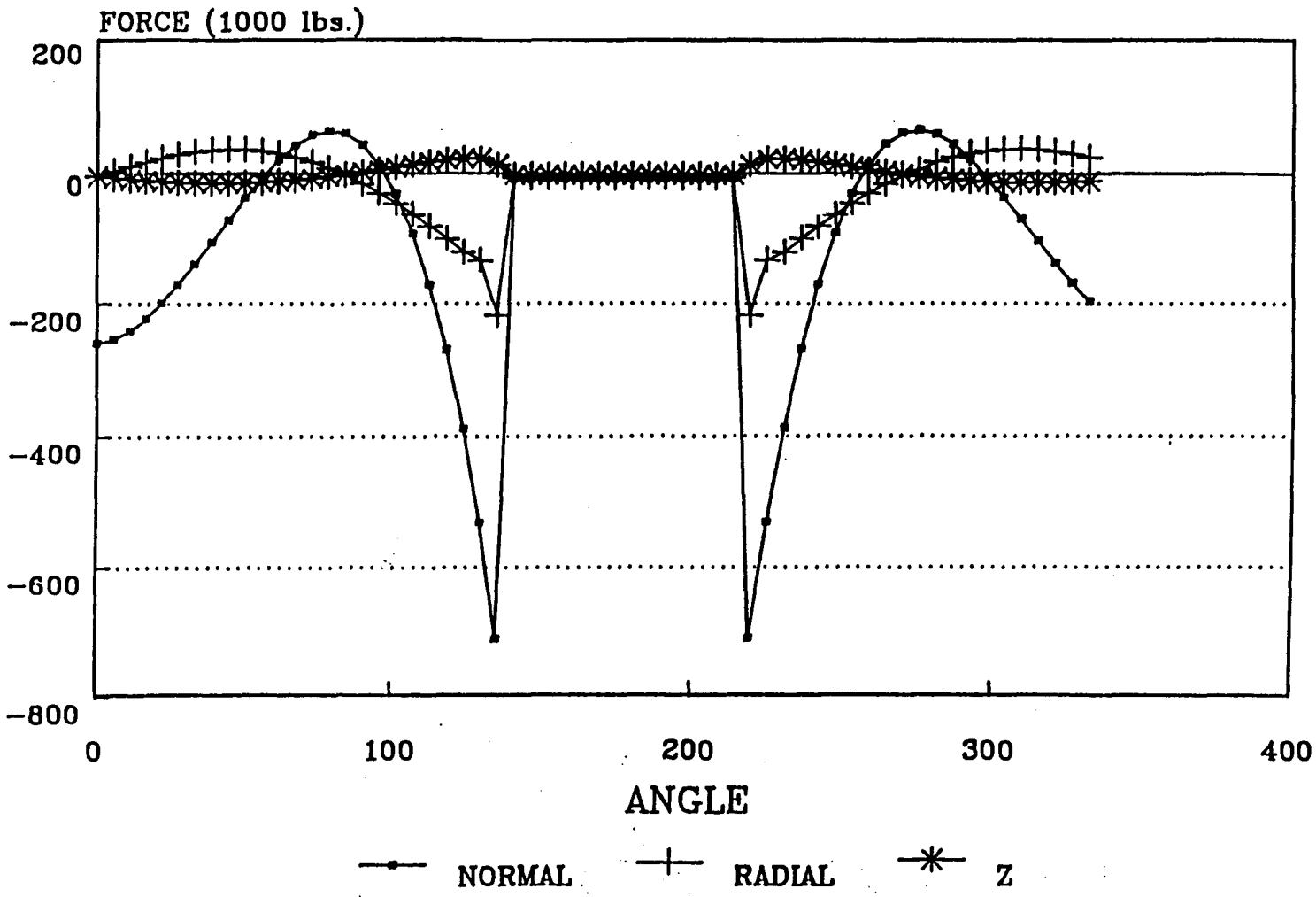

Figure 5

HAC1 – HAC2 BOUNDARY

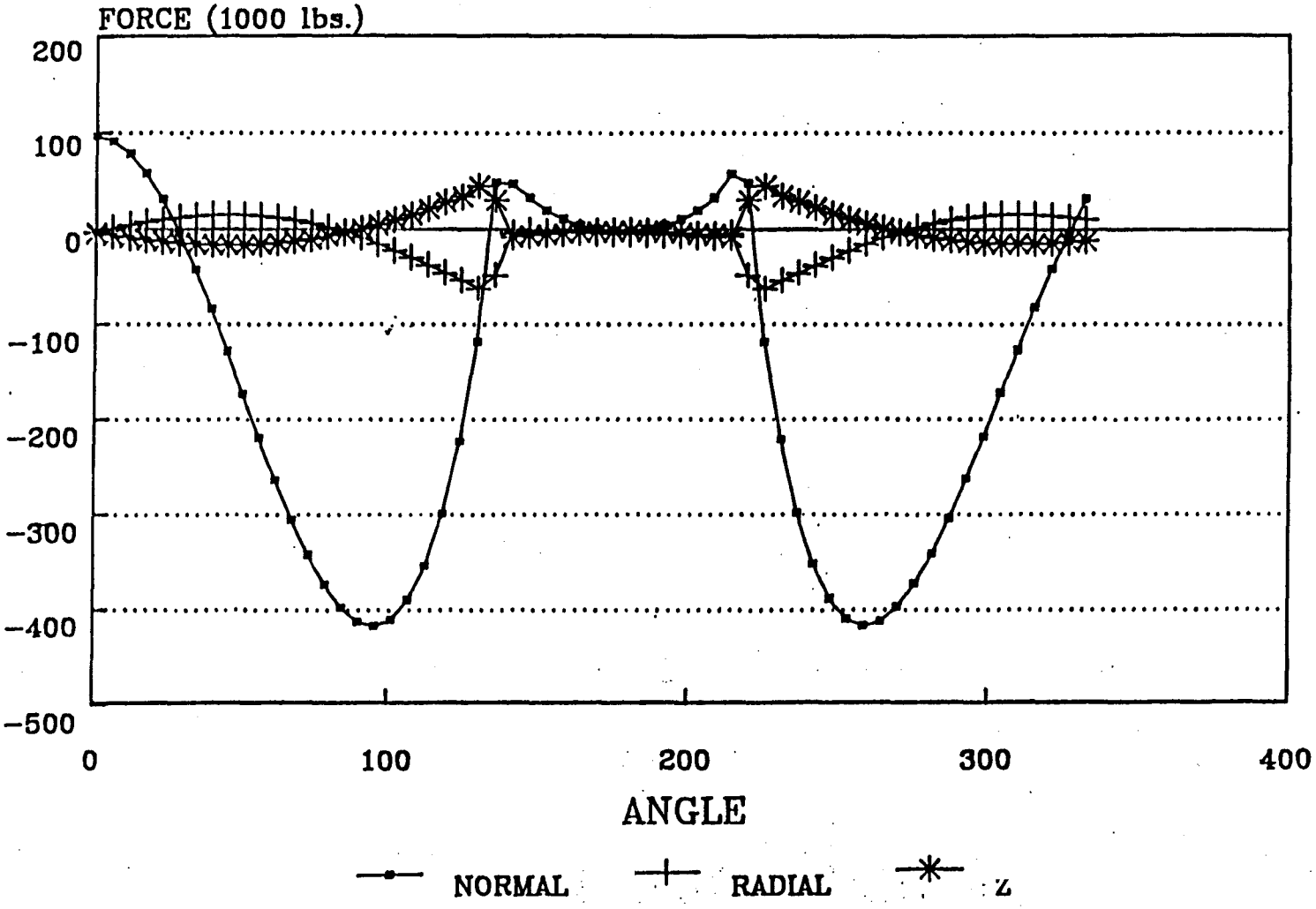

Figure 6

EM – HAC1 BOUNDARY

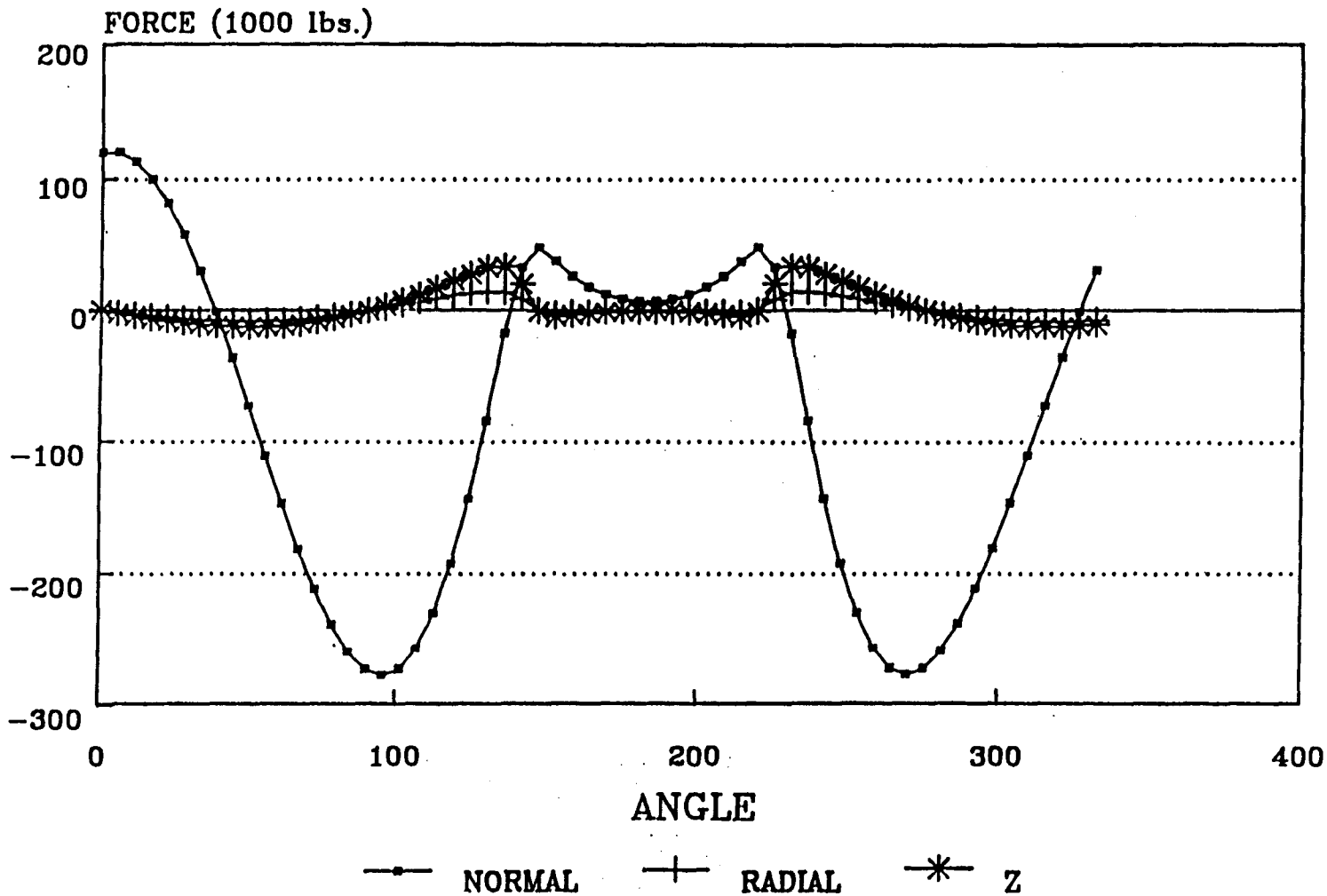

Figure 7

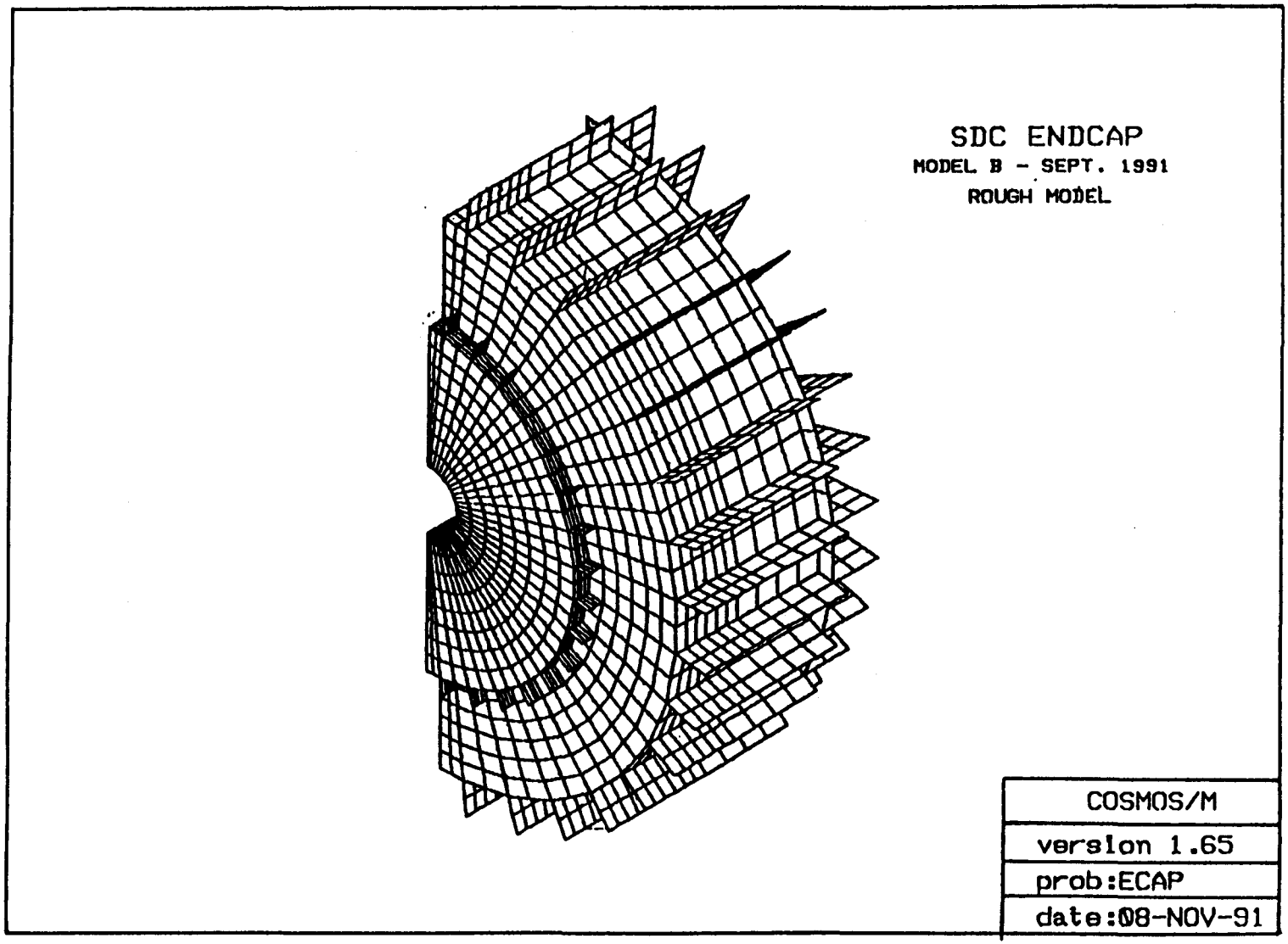
SDC ENDCAP
MODEL B - SEPT. 1991
ROUGH MODEL
COSMOS/M
version 1.65
prob:ECAP
date:08-NOV-91

Figure 8

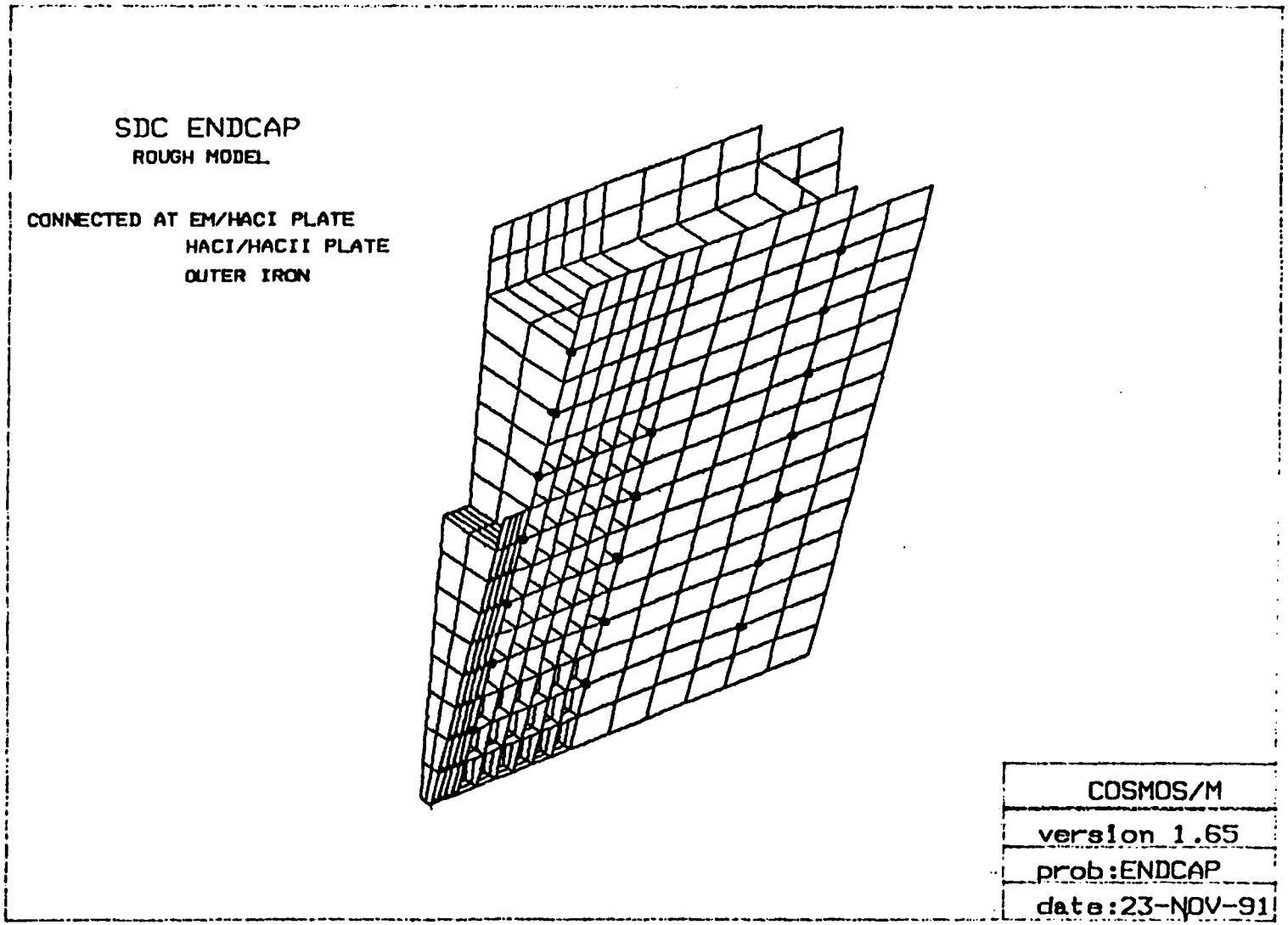
SDC ENDCAP
ROUGH MODEL
CONNECTED AT EM/HACI PLATE
HACI/HACII PLATE
OUTER IRON
COSMOS/M
version 1.65
prob:ENDCAP
date:23-NOV-91

Figure 9

Endcap Connecting Forces

EMC – HAC I Plate

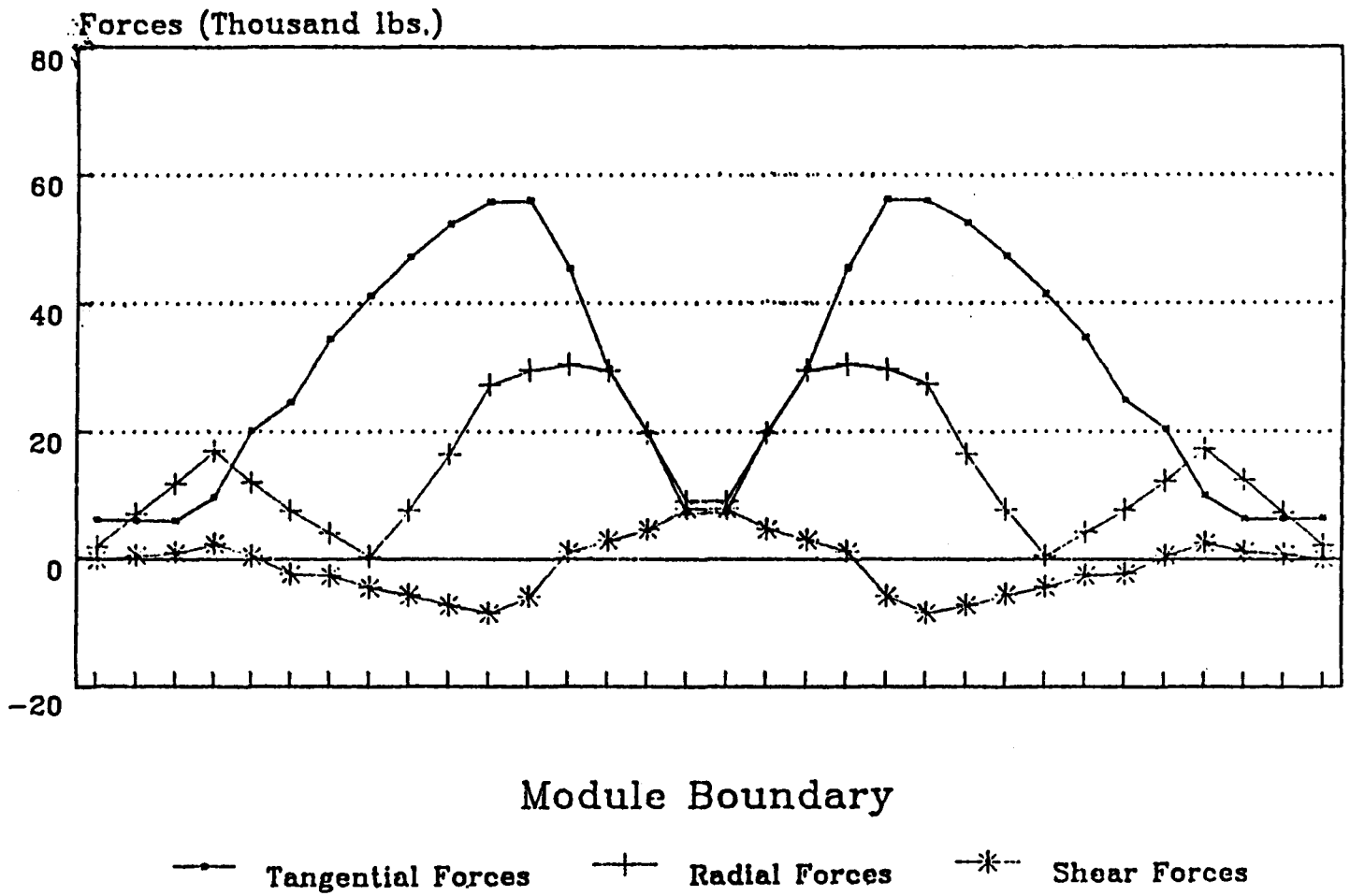

Figure 10

8. LOS ALAMOS NATIONAL LABORATORY (LANL)

Cost and Schedule Activities

Provisions to the program plan for the silicon tracking system are continuing. Task definition in accordance with the work breakdown structure is nearly complete. The revised program plan will be translated in OPEN PLAN format by the end of December. Modifications to the program plan will require revisions to the resource inputs to the CUE scheduler program. This cost information is being prepared. We also are generating design information drawings for vendors to use in preparing their construction quotes. Rough order of magnitude cost estimates are being solicited for the space frame and central cooling rings. Drawings are being prepared for the forward cooling rings and support structure as well as the inner and outer enclosures. Ultimately, all major components will be formally bid by vendors and/or in-house fabricators.

Structural Analysis Studies

Finite element calculations are in progress to determine the sensitivity of the silicon shells to asymmetric thermal loads. The initial model is that of a single 420-micron outer-diameter cooling ring without silicon chips. Boundary conditions used in this model simulate the three point 2-2-2 kinematic mounting scheme being considered for the shell support design. A symmetric, linearly varying temperature distribution is applied to the central half of one of the 1200 arc segments to simulate a thermal load. Initial results indicated that for a temperature distribution ranging from a reference temperature of 0 degrees C to a maximum of 12 degrees C, the in plane displacements are on the order of several microns. Axial, or out off plane displacements are several orders of magnitude less and appear to be negligibly small. Future models will include totally asymmetric temperature distributions around the entire ring as well as models bearing silicon chips.

Radiation Length Studies

Radiation length studies, based on RTRACE, a package within the SDCSIM simulation shell, have advanced significantly. IN addition to calculating radiation length, nuclear absorption length, and geometric extent of materials as a function of rapidity and phi, RTRACE has been enhanced to calculate these quantities for everything in front of a material. It also calculates the measurement lever arm of detector systems both in r and z. I now allows for a smeared and/or offset vertex, and will make tables of any calculated quantity with any granularity. Preliminary calculations of the radiation length of the silicon tracking system as a function of rapidity show variations from 3.8% at zero rapidity to a maximum of 7-8% around a rapidity of 1.3, depending on the details of the geometry modeled. These simulations include the silicon detectors, support structures including the metal matrix composite space frame, the enclosure vessel, the beam pipe, the cooling ring and wick, the electronics package, and the local power distribution system. These studies will continue and will be helpful in finding the final detector configuration.

Materials Science Studies

Physical testing to quantify the mechanical properties of the graphite fiber/cyanate ester resin composite materials system envisioned for use in the silicon tracking system continues. A parallel program for improving the thermal performance of these materials in critical applications such as the cooling rings is also underway. To promote a near isothermal structure, free from thermal distortions, the compression-molded cooling rings must have high, nearly isotropic thermal conductivity. The two methods being considered for achieving

this objective are the addition of high thermal conductivity materials to the fiber/resin system, and preferential fiber orientation while molding. A test matrix for thermal conductivity enhancement via resin filling may be found as Table 1. Another prospect for thermal performance enhancement involves a unique, highly developmental perform manufacturing process. Contracts for evaluating the coefficients of thermal and moisture expansion for our materials system are being written. The sagacity of choosing a hydrophobic, cyanate ester resin is expected to be confirmed by these tests which will be conducted during January of 1992. The results of these tests will clearly define the materials parameters available for use in the detector. Based upon this knowledge, accurate design study input and a valid benchmark for the system's stability can be established.

Table 1: Filled-Resin Thermal Conductivity Enhancement Test Matrix (Values in Wt. %)

P-75 Graphite Fibers (100-μm-long	Cyanate Ester Resin (Type 954-3)	Carbon Particles (~12μm diam)	Aluminum Nitride Particles (~10μm diam)
---	100†	---	---
---	90	10	---
---	80	20	---
---	50	50	---
---	90	---	10
---	90	---	20
---	50	---	50
60†	40	---	---
50	40	10	---
40	40	20	---
20	30	50	---
50	40	---	10
40	40	---	20
20	30	---	50

† Denotes control formulation.

Note: Three samples of each formulation are being fabricated. A total of 42 speciments will be tested.

Alignment Studies

The alignment maintenance system, an important and challenging system for the calibrated detector, monitors detector alignment drift between calibration runs. This is an especially important operational system, because calibration is likely to be a time consuming activity.

We believe it will be possible to continuously monitor 3-D positions of subassemblies relative to one another, and the position of the silicon detector relative to the outside world, with a compact, non-intrusive fiber optic motion sensor. As shells are built into an assembly, a 7-fiber speckle-pattern motion sensor will be attached at each end of every other shell to monitor 3-D motions of the previous shell in the assembly. Alignment status will be built-up from the inner shell to the outer shells and to the reference system outside the detector. Using this technique, alignment status can be continually monitored form initial assembly through transport and installation, and during operational use between calibrations.

The fiber optic motion sensor is not a research device not commercially available. This technique requires research to develop the concept into a reliable instrument and to test and calibrate it during shell prototype tests. There is no other practical technique to continuously monitor the alignment status of the detector during transport and between calibrations.

9. ICF - KAISER ENGINEERS (KE)

Efforts continued on the conceptual design and the criteria for construction and support of the Forward Toroids for the Descoped Detector and made a presentation at the SDC engineering integration meeting on November 11-12, in Dallas.

The descoped Forward Toroids could be built from a total of 64 blocks, instead of the 96 blocks of the Baseline Forward Toroids. this will simplify and shorten construction time which will further reduce costs.

Conceptual designs of a rotating roller support system was developed, as well as a two-piece removable transfer frame to be installed between the end of the barrel and the operating floor to support the Forward toroids during assembly or disassembly of the detector. In the future these designs will be refined and fully coordinated with the Forward Toroid muon system.

There was no activity this month on the Construction Planning of the detector pending finalization of the Descoped Detector design criteria and the negotiation of additional funding.

10. LAWRENCE BERKELEY LABORATORY

Computing Systems

Most activity has been associated with the writing of the Offline Computing section of the SDC Technical Proposal. There was a four-day Computing Group Workshop meeting in Dallas followed a week later by the SDC Meeting. Much of the time in between was devoted to writing text for the Proposal Draft.

The RS/6000 communications problem is temporarily solved with prospects for a permanent solution. For the time being, we have borrowed an older model of the IBM Ethernet card which does not cause the problem with the Cisco router box. The latest word from IBM is that, while they maintain that it is Cisco which is not following the Ethernet standard, nevertheless IBM will produce a newer version of the card which works with the router. These cards should be available in early '92, and the local technical representative has promised a replacement as soon as possible.

A new version of ObjectStore arrived. Its behavior for large databases is significantly improved. I have enclosed comparision plots of the database load times for the previous best configuration and for the same configuration with the new ObjectStore. There is about a 35% decrease in overall load time and a considerably shallower, although not vanishing, curvature.

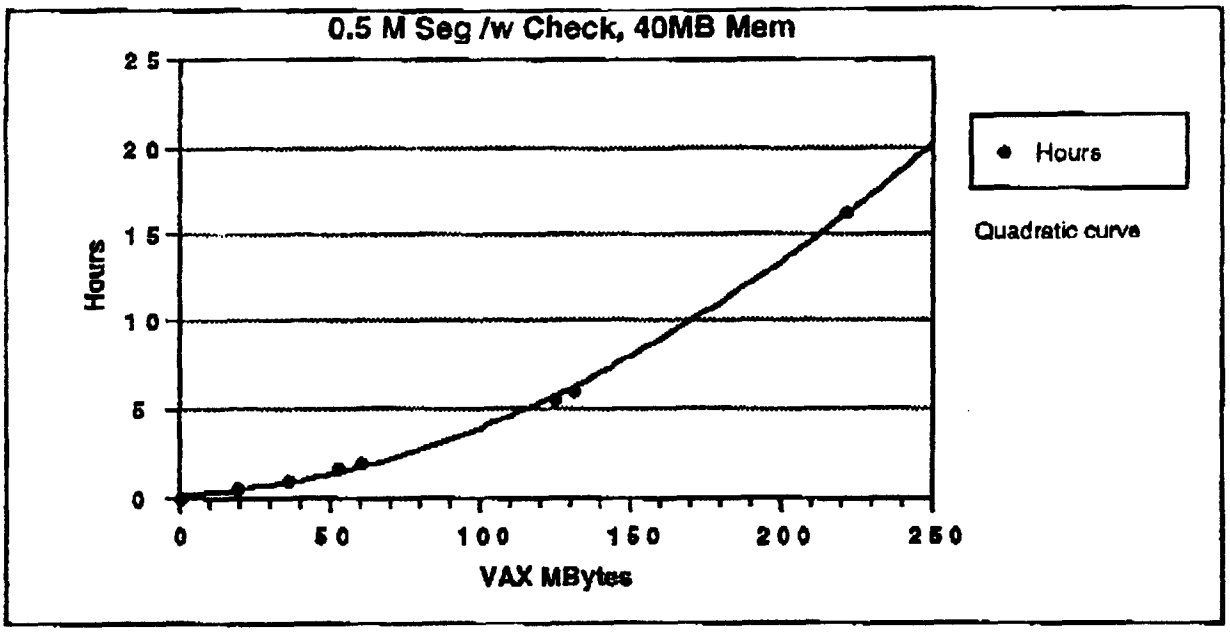

Previous Best

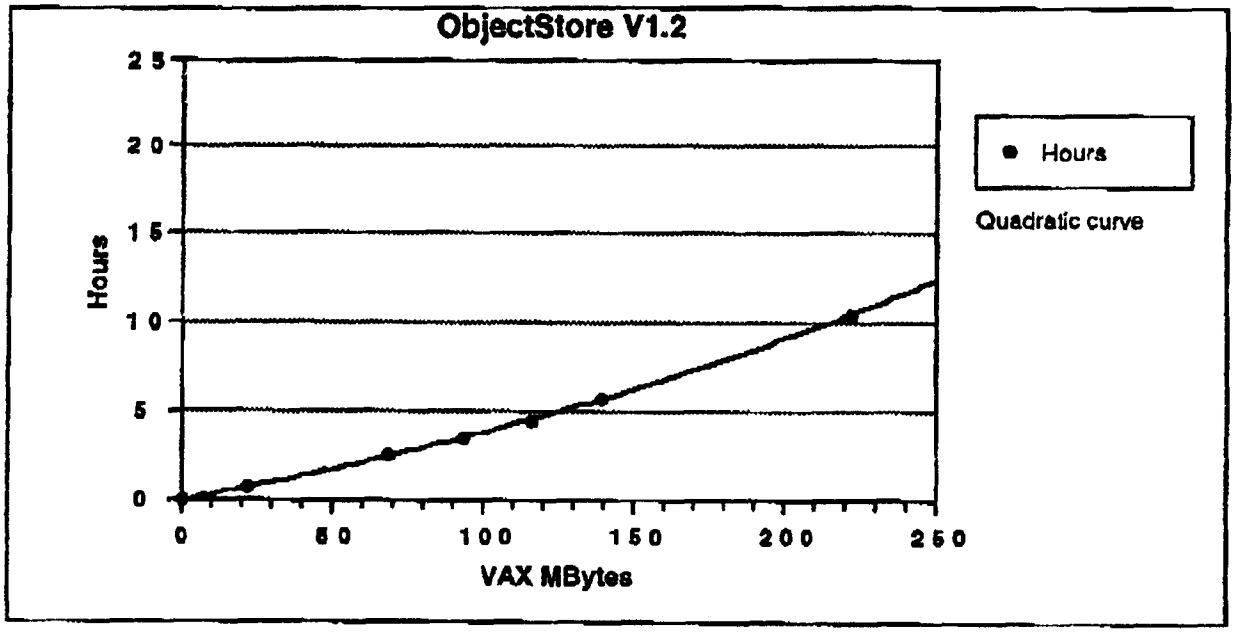

New ObjectStore release

16. MARTIN MARIETTA

Muon System Costing and Scheduling Phase II

Task Accomplishments

1. Reviewed the documentation received from the muon system cost and schedule kick-off meeting in October and incorporated the data into the muon system cost spreadsheets for the four muon chamber concepts.

2. Developed a bottoms-up cost estimate for the central barrel muon steel based on the specifications delivered to the USSR. This estimate was given to Jim Bensinger for comparison with USSR estimates.

3. Updated the muon system cost parametrics for barrel torroid radius and length and the impacts on the cost of the entire muon system.

4. Developed SDC muon system coverage plot of lever arm versus eta.

5. Obtained preliminary design reports for the four muon chamber concepts.

6. Developed total muon system cost estimates with Jim Bensinger for alternative detector configurations being considered.

7. Developed a cost breakdown for the barrel coils. A bottoms-up methodology for costing of the coils is currently under development. Preliminary design and manufacturing concepts have been collected and are being incorporated into the bottoms-up cost estimate.

8. Developed the total muon system cost estimate for incorporation into the SDC detector roll-up scheduled on 27 Nov.

9. Continued to update and enhance the muon subsystem time-phased network with inputs from the subsystem working groups and Martin Marietta Industrial Engineering. Resource loaded the Open Plan muon system network and provided database to SSCL in support of the 27 Nov cost and schedule roll-up.

10. Developed manufacturing flows for the Washington muon system concept, including options with and without field shaping, at the drift cell assembly and detail levels. Created a "straw man" parts list to aid in the development of the flows, tool lists, and manufacturing process definitions. Created a tool list with design and fabrication estimates to support the two concepts and the development of the manufacturing process estimates. Developed detail part, subassembly, and drift cell assembly manufacturing processes and estimates for both options. Started work on flows for the module and super module assemblies. Started estimates on the module assembly details and the assembly of the module.

11. Developed the site assembly flow, tooling requirements, level-of-effort manpower requirements, skill mix, facility needs, and floor layout to support cost, resource, and schedule analyses of the Wisconsin muon system concept.

12. Attended and supported the following meetings at SSCL:
    - SDC Collaboration meetings 14-15 Nov.

- Muon chamber review committee kick-off meeting 14-15 Nov.

Deliverables Submitted to the SSCL:

1. SDC central muon steel bottoms-up cost estimate for comparison to the USSR estimate.

2. SDC muon system cost estimate.\

3. Muon system cost sensitivities.

4. SDC muon system lever arm vs eta plot.

5. Muon chamber cost estimates for four concepts.

6. Time-phased resource-loaded Open Plan muon system network updated from baseline version produced for Phase I of this contract.

7. Manufacturing operations labor estimates for four chamber concepts.

Engineering Services

Task Accomplishments:

1. Reviewed the draft of the SDC Costing and Scheduling Procedures for the Technical Proposal document and provided additional information to be included in the published version (issued 15 Nov).

2. Assisted the Cost/Schedule Integration Manager at SSCL in the cost roll-up for the entire detector to be issued 27 Nov.

3. Assisted the Cost/Schedule Integration Manager at SSCL in schedule roll-up database integration using the SSCL PMO LAN Open Plan system, 25-27 Nov.

4. Performed initial resource allocation modeling (RAM) for the Wisconsin muon system concept. Presented results to T. Prosapio and Wisconsin proponents.

5. Determined the ratio of magnetic bend angle to multiple scattering angle for the 18 Nov. baseline configuration of the SDC muon system using automated ray tracing through a solid model.

6. Surveyed requirements for detector installation support equipment and collected installation data.

7. Revised and updated detector installation flows and schedules.

8. Supported definition of detector alignment requirements leading to an alignment allocation matrix.

9. Defined options to muon chamber sizing and placement for improved muon detection coverage.

10. Attended and supported the following meetings at SSCL:
    - Tracking chamber review committee meeting, 14-15 Nov.

- Cost and schedule integration kickoff meeting, 13-14 Nov.
- SDC collaboration meeting, 13-15 Nov.
- SDC detector and muon system integration meetings including those on 11-12 Nov.
- Muon system alignment meeting, 12 Nov.

Deliverables Submitted to the SSCL

1. Cost and schedule data packages for the SDC cost/schedule roll-up of 27 Nov.

2. Initial RAM results for the Wisconsin muon system concept .

3. Plots of the ratio of magnetic bend angle to multiple scattering angle for the 18 Nov configuration of the SDC muon system.

B. PROGRAM COSTS

The budgets indicated below are for FY91 "post-LoI" funds allocated Apr. 1991 and Aug.-Oct. 1991.

Institution	Budget K$	November Cost (Actual or Estimated)	Prior Months (actual cost) K$	Total Cost $
1. ORNL	210	—	—	—
2. PSL - Muon	80	12.1	15.3	27.4
3. PSL-Trigger	75	21.6	34.2	55.8
4. FNAL				
A. SC Solenoid	393	113.5	434.2	547.7
B. Calorimetry	159	40.0	146.9	186.8
C. Data Acq. Sys.	50	9.0	22.4	31.4
D. Muon	93	5.0	19.8	24.8
E. Fiber Tracker Read-out	95	0.2	0.1	0.3
F. Calorimeter Electronics	65	0	132.7	132.7
G. Calorimeter Engineering	100	36.0	0	36.0
5. ANL	230	31.1	111.7	143.0
6. WSTC	123	0	123.0	123.0
7. U. MICHIGAN	83	0	0	0
8. LANL	150	NA	135.0	NA
9. KE	210	7.4	197.1	204.5
10. LBL				
A. Integration & Mgmt.	673	N/A	821.1	N/A
b. Liq. A Calorimetry	0	N/A	221.4	N/A
C. Silicon Tracker	72	N/A	72.9	N/A
D. Computing Systems	119	N/A	128.7	N/A
E. Calorimetry Electronics	25	N/A	44.5	N/A
F. Contract Costs	53	–0	53.0	53.0
11. IBM	35	—	—	—
12. U. CHICAGO	47	—	—	—
13. HARVARD	47	—	—	—
14. U. PENNSYLVANIA	62	—	—	—
15. SANDIA	38	—	—	—
16. MARTIN MARIETTA		55.4	89.4	144.8

SDC Note SDC-91-00140
December 4, 1991

SDC Jet Trigger Studies

W. Temple, J. Lackey, T. Gorski, W.H. Smith
University of Wisconsin

1 Introduction

A major requirement of the SDC First Level Trigger is the detection of jets. Jet detection is important for the top quark signal, and quark compositeness searches. The jet p_T threshold needs to be set so that there is a 1-2 decade overlap in data with that from other experiments (for example, CDF)[3]. The jet trigger is based on calorimeter information[4]. The basic unit of calorimeter level 1 trigger information is the trigger tower. This is the sum of either the energy in the calorimeter electromagnetic (EM) or hadronic (HAC) compartment in a $.1\eta \times .1\phi$ region. Generally, this is composed of the transverse sum of 4 .05 x .05 EM towers or the longitudinal sum of two .1 x .1 HAC towers digitized on an 8-bit logarithmic scale. This information is sent by the calorimeter front end electronics to the level 1 trigger crates[5]. The information is received by the calorimeter isolaton/summation crates[1]. These sum up the energy in .4 x .4 regions. At this point there is the option to test the the energy in the .4 x .4 towers against a series of thresholds, as well as summing up these .4 x .4 sums an array of .8 x .8 sums, or two overlapping arrays of .8 x .8 sums. The purpose of this document is to investigate what strategy is best for triggering given the calorimeter information that is available. This includes calculating the effects of the digitization scale and the methods by which towers are combined and tested. In summary, the performance of jet triggers for the SDC was studied to answer the following questions:

- What size grid is optimal for finding jets?
- Should two overlapping grids or one non-overlapping grid of jet towers be used?
- What type of integer scale for energies gives the best resolution?

We used 64000 QCD twojet events from 20-400 GeV, and minbias events corresponding to a poisson distribution with mean 1.6 events per crossing were generated using the Monte Carlo program ISAJET. The events were integrated over three beam crossings, using a scintillator calorimeter shaping function from ZEUS. The energy deposit in the calorimeter which resulted was simulated by the program SIM3, from Greg Sullivan at the University of Chicago. Jets were looked for on three size scales, with energies first converted to one of two possible integer scales. A trigger tower size of .1x.1 in η and ϕ was used for η <2, and twice that for η >2. The simulation was run on Symmetric MultiProcessor Silicon Graphics Inc. 4D/380s at the Physics Detector Simulation Facility of the SSC Laboratory.

Jets were looked for in a calorimeter covering $\eta < 3$. Energy sums were made in each square in two sorts of grids – an overlapping grid, so that the calorimeter was covered twice,

Type of jet trigger		logarithmic scale 1 kHz	logarithmic scale 3 kHz	semi-linear scale 1 kHz	semi-linear scale 3 kHz
.2x.2	non-overlapping	107	78	107	78
.2x.2	overlapping	115	83	114	83
.4x.4	non-overlapping	130	95	128	95
.4x.4	overlapping	139	102	138	102
.8x.8	non-overlapping	148	110	147	109
.8x.8	overlapping	158	117	156	116
1.6x1.6	non-overlapping	165	123	164	122
1.6x1.6	overlapping	175	132	174	131

Table 1: Jet E_t threshold needed to achieve given rates (GeV)

and a non-overlapping grid. The sizes of grids used were .2x.2, .4x.4, .8x.8, and 1.6x1.6 squares in $\eta \times \phi$. The simulation did not exactly duplicate the electronics setup beyond the local level, but instead converted the E_t in each trigger tower to an 8-bit logarithmic scale and back to a real number before adding. This implementation is based on [1]. As an alternative scale a 9-bit semi-linear scale was used, which consisted of two overlapping 8-bit linear scales with one bit indicating range. For each size of regions searched, both a single array of non-overlapping sums and two overlapping arrays were used.

The electronics for testing on a larger a jet tower size is simpler, since each step in size results in a reduction by four times of the final number of pieces of information which must be compared. In a sense, overlapping grids of a given size are of similar difficulty as non-overlapping grids of the next smaller size, since the information required to form two overlapping grids of, say, .8x.8 towers, is just the information required to find one non-overlapping grid of .4x.4 towers. However, a single grid involves less electronics than two grids. Also, the number of bits required to transmit the energy of a trigger tower must be as small as possible to give good jet resolution, but is limited by the need to have better resolution at lower E_t values for electron identification. The 8-bit logarithmic scale allows transmission of the HAC and EM energy every 16 nsec on a 1 Gbit/sec optical fiber [5, 1]. A 9-bit scale would not allow this. The 8-bit logarithmic scale used here was also used to give the electron trigger efficiencies given in [2].

2 Jet Rates

All rates here are shown in kHz, where a 1 mb jet cross section corresponds to 1 MHz at the SSC design luminosity of $10^{33} cm^{-2} sec^{-1}$. Table 1 shows the E_t thresholds necessary to achieve trigger rates of 1 and 3 kHz. For instance, if one wanted to have a background rate of 3 kHz using a non-overlapping grid of .4x.4 jet towers and a logarithmic scale, the required E_t threshold would be 95 GeV. Figure 0 shows the rates plotted against E_t threshold for overlapping and non-overlapping grids of all four tower sizes.

In Figures 1-6, the trigger uses an 8-bit logarithmic scale. Figure 1 shows the rates

plotted versus E_t threshold for the four jet tower sizes, using non-overlapping jet towers. We see that the proportional difference in rates between small and large jet tower sizes increases with the E_t threshold. This would seem to indicate that the higher energy jets would be less likely to be confined in small regions of the calorimeter. Figure 2 shows the rates plotted versus E_t threshold for the four jet tower sizes, using two overlapping grids of towers. The same widening occurs with increasing threshold, suggesting that at sizes less than 1.6x1.6, using overlapping grids does not suffice to ensure that all jets are contained. Figures 0-2 are comparable to Figure 2 in [3].

Figure 3 shows the rates for .2x.2 jet towers, comparing overlapping and non-overlapping towers. Figure 4 compares rates for overlapping and non-overlapping .4x.4 jet towers. Figure 5 shows these rates for .8x.8 towers. Figure 6 shows the rates for 1.6x1.6 towers. With all four tower sizes, we see that the rate difference between overlapping and non-overlapping towers grows with the E_t threshold.

Figure 7 shows the rates for .8x.8 overlapping grids of jet towers, comparing the 8-bit logarithmic scale to the 9-bit semi-linear scale. This indicates that the semi-linear scale perhaps loses some efficiency at high energies. The semi-linear scale used covers a broader range than does the logarithmic scale; while the logarithmic scale uses 8 bits to go from .5 GeV to 500 GeV, the semi-linear scale goes from .3 GeV to 76 GeV on one linear scale, and from 20 GeV to 1000 GeV on the other. This uses 9 bits, so the scale range per bit is not very different. This particular semi-linear scale shows no clear advantage.

3 Jet Trigger Efficiencies

For measuring jet trigger efficiency, events with actual jet rapidity greater than 2.8 were ignored to ensure that only jets within the fiducial volume of the calorimeter were considered.

First the effect of using a two overlapping grids rather than one non-overlapping grid was determined. Figure 8 shows the efficiency curve for .2x.2 jet towers, plotted against the p_t of the highest p_t jet in the event, for both non-overlapping and overlapping jet towers. The threshold here was set to achieve a 3 kHz rate: for overlapping grids of towers, the required threshold was 83 GeV; for a non-overlapping grid the threshold was 78 GeV. We see that the lower jet threshold used by the non-overlapping jet trigger only results in significantly higher efficiency in a very narrow threshold range – this is due to the steeply falling distribution of jet energies. Figure 9 compares efficiency of .4x.4 overlapping and non-overlapping jet towers with a 3 kHz rate. A 102 GeV E_t threshold was needed for overlapping grids of towers, while a 95 GeV threshold suffices for a non-overlapping grid. Again, the efficiency turn-on is considerably sharper for the overlapping grids of towers, and compensates for the higher threshold. Figure 10 shows efficiency for .8x.8 overlapping and non-overlapping jet towers with a 3 kHz rate. Here thresholds of 110 and 117 GeV sufficed to achieve a 3 kHz rate using non-overlapping and overlapping grids, respectively. The efficiency for 1.6x.16 overlapping and non-overlapping grids is shown in Figure 11. Here, thresholds of 132 and 123 GeV were required for a rate of 3 kHz.

If we set the threshold to get a 1 kHz rate, .2x.2 jet towers would give the efficiency shown in Figure 12. However, at this rate, both the overlapping and non-overlapping efficiencies

have not reached full efficiency by 400 GeV p_t. This is with E_t thresholds of 115 and 107 GeV, respectively. High-energy jets tend to deposit their energies over a much larger area than .2x.2. Figure 13 compares efficiency of .4x.4 overlapping and non-overlapping jet towers with a 1 kHz rate. Here, thresholds of 139 and 130 GeV respectively were required for a rate of 1 kHz. Figure 14 shows efficiency for .8x.8 overlapping and non-overlapping jet towers with a 1 kHz rate. Thresholds of 158 and 148 GeV respectively were required for a rate of 1 kHz. The corresponding efficiency for 1.6x1.6 overlapping and non-overlapping grids of jet towers is shown in Figure 15. Thresholds of 175 and 165 GeV were required for a rate of 1 kHz.

We have examined the effect tower size has on efficiency for non-overlapping towers. Figure 16 shows the efficiency for non-overlapping towers for all four tower sizes, with thresholds set for a 3 kHz rate. The thresholds which give a 3 kHz rate are 123 GeV for 1.6x1.6, 110 GeV for .8x.8, 95 GeV for .4x.4, and 78 GeV for .2x.2. Though the differences in thresholds for this rate are large, the efficiency curve for .2x.2 towers has not reached 20% when it is passed by the efficiency for .4x.4 towers. Likewise, 1.6x1.6 towers outperform the smaller sizes by the time they have reached approximately 40% efficiency. Figure 17 compares the efficiencies for the tower sizes, with thresholds set to achieve a 1 kHz rate. The thresholds needed are 132 GeV for 1.6x1.6 towers, 117 GeV for .8x.8 towers, 102 GeV for .4x.4 towers, and 83 GeV for .2x.2 towers. At this rate, the efficiencies are similar for the three smaller sizes at a jet p_t of 160 GeV, where the efficiency is about 16%; beyond 200 GeV the 1.6x1.6 size performs best.

We have examined the effect tower size has on efficiency for overlapping towers. Figure 18 shows the efficiency for overlapping towers for all four tower sizes, with thresholds set for a 3 kHz rate. The thresholds needed are 165 GeV for 1.6x1.6 towers, 148 GeV for .8x.8 towers, 130 GeV for .4x.4 towers, and 107 GeV for .2x.2 towers. Figure 19 compares the efficiencies for overlapping grids with the different tower sizes and a 1 kHz rate. The thresholds which give a 1 kHz rate are 175 GeV for 1.6x1.6, 158 GeV for .8x.8, 139 GeV for .4x.4, and 115 GeV for .2x.2. The differences between different tower sizes seem to be the same in character with overlapping towers as they were with non-overlapping towers.

Table 2 presents similar information in a slightly different format. If we try to achieve a given rate, the question is asked, at what jet p_t do we achieve 75% efficiency? The efficiency in question is efficiency in finding all the events with actual jet $p_t \geq$ the given p_t. The results are shown for each jet tower size, both non-overlapping and overlapping, using the 8-bit logarithmic scale and the semi-linear scale. Tables 3, 4, 5, and 6 show the jet p_t values required to reach 85%, 90%, 95%, and 98% efficiency,respectively. Each of the efficiencies considered is reached at the lowest p_t by overlapping grids of 1.6x1.6 towers. The higher efficiency demanded, the more distinct is this effect.

With respect to the two scales used, the difference in efficiency noted using the two scales is not very large; certainly it is a much smaller effect than those of changing grid size or from non-overlapping to overlapping. Thus it seems likely that the difference between these two scales for energy digitization is not a particularly important issue.

Type of jet trigger		logarithmic scale 1 kHz	logarithmic scale 3 kHz	semi-linear scale 1 kHz	semi-linear scale 3 kHz
.2x.2	non-overlapping	226	173	228	174
.2x.2	overlapping	218	167	217	167
.4x.4	non-overlapping	214	162	213	163
.4x.4	overlapping	204	154	205	154
.8x.8	non-overlapping	202	153	203	152
.8x.8	overlapping	195	149	194	149
1.6x1.6	non-overlapping	195	148	195	146
1.6x1.6	overlapping	191	145	190	143

Table 2: Jet p_t at which 75% efficiency is reached (GeV)

4 Conclusions

For each of the efficiency levels considered, the largest jet tower size is the most successful, and overlapping towers are more successful than non-overlapping towers. The inherent disadvantage of large jet trigger towers, that they are so large as to let in phenomena which are not jets, seems to be more than compensated for by the falling rates at high jet p_t. This conclusion is reached in the context of the present simulation. As the simulation evolves, this investigation will continue. At present, the best results are found by use of a trigger design with overlapping grids of 1.6x1.6 towers for the primary trigger. However, it is possible that with higher luminosity or a better calorimeter simulation, this size will present disadvantages. It seems possible, then, that a jet trigger might use overlapping grids of .8x.8 towers for the primary jet trigger and a prescaled trigger on a non-overlapping .4x.4 grid of towers at a much lower threshold, or something similar. We also conclude that the 8-bit logarithmic scale shows at least as good performance as does the 9-bit semi-linear scale of two 8-bit linear ranges, and that quite possibly any similar 8 or 9-bit scale would give roughly the same results.

References

[1] T. Gorski, J. Lackey, W.H. Smith, *Level 1 Trigger Decision Design for the SDC*, SDC Note SDC-91-00088, 1991.

[2] W.H. Smith, J. Lackey, T. Gorski, W. Temple, *Isolated Electron Pattern Logic Design and Performance at the SSC*, SDC Note SDC-91-00087, 1991.

[3] A. Lankford, et al., *Conceptual Design of the SDC Trigger from the SDC Trigger Group*, SDC note SDC-91-00098, 1991.

[4] T. Gorski, J. Lackey, W.H. Smith, W. Temple, *Isolated Electron Pattern Logic Design and Performance at the SSC*, SDC Note SDC-91-00087, 1991.

Type of jet trigger		logarithmic scale 1 kHz	logarithmic scale 3 kHz	semi-linear scale 1 kHz	semi-linear scale 3 kHz
.2x.2	non-overlapping	262	200	262	199
.2x.2	overlapping	250	187	250	187
.4x.4	non-overlapping	246	184	245	185
.4x.4	overlapping	230	171	231	171
.8x.8	non-overlapping	227	168	228	168
.8x.8	overlapping	215	163	214	163
1.6x1.6	non-overlapping	214	162	214	160
1.6x1.6	overlapping	204	156	204	155

Table 3: Jet p_t at which 85% efficiency is reached (GeV)

Type of jet trigger		logarithmic scale 1 kHz	logarithmic scale 3 kHz	semi-linear scale 1 kHz	semi-linear scale 3 kHz
.2x.2	non-overlapping	291	220	292	220
.2x.2	overlapping	279	210	278	210
.4x.4	non-overlapping	270	203	265	204
.4x.4	overlapping	252	185	252	185
.8x.8	non-overlapping	248	184	251	182
.8x.8	overlapping	231	174	231	174
1.6x1.6	non-overlapping	231	171	231	169
1.6x1.6	overlapping	214	164	214	162

Table 4: Jet p_t at which 90% efficiency is reached (GeV)

Type of jet trigger		logarithmic scale 1 kHz	logarithmic scale 3 kHz	semi-linear scale 1 kHz	semi-linear scale 3 kHz
.2x.2	non-overlapping	358	257	363	257
.2x.2	overlapping	330	244	330	244
.4x.4	non-overlapping	311	234	311	235
.4x.4	overlapping	290	214	293	215
.8x.8	non-overlapping	286	214	289	213
.8x.8	overlapping	262	193	262	193
1.6x1.6	non-overlapping	266	193	265	192
1.6x1.6	overlapping	235	177	235	175

Table 5: Jet p_t at which 95% efficiency is reached (GeV)

Type of jet trigger		logarithmic scale 1 kHz	logarithmic scale 3 kHz	semi-linear scale 1 kHz	semi-linear scale 3 kHz
.2x.2	non-overlapping	> 400	296	> 400	302
.2x.2	overlapping	> 400	289	> 400	288
.4x.4	non-overlapping	377	269	370	270
.4x.4	overlapping	354	253	354	253
.8x.8	non-overlapping	349	252	349	252
.8x.8	overlapping	310	228	308	228
1.6x1.6	non-overlapping	295	226	300	225
1.6x1.6	overlapping	269	199	269	195

Table 6: Jet p_t at which 98% efficiency is reached (GeV)

[5] W. H. Smith, T. Gorski, J. Lackey, *SDC Trigger Preliminary Conceptual Design*, SDC Note SDC-91-00089, 1991.

[6] G. Sullivan and M. Miller, *Calorimetry trigger rates at the SDC*, U. Chicago SDC note SDC-91-00099, 1991.

[7] Zeus Collaboration, *Status Report 1989*, DESY, Hamburg, Germany, 1989, Fig. 5.8.10.

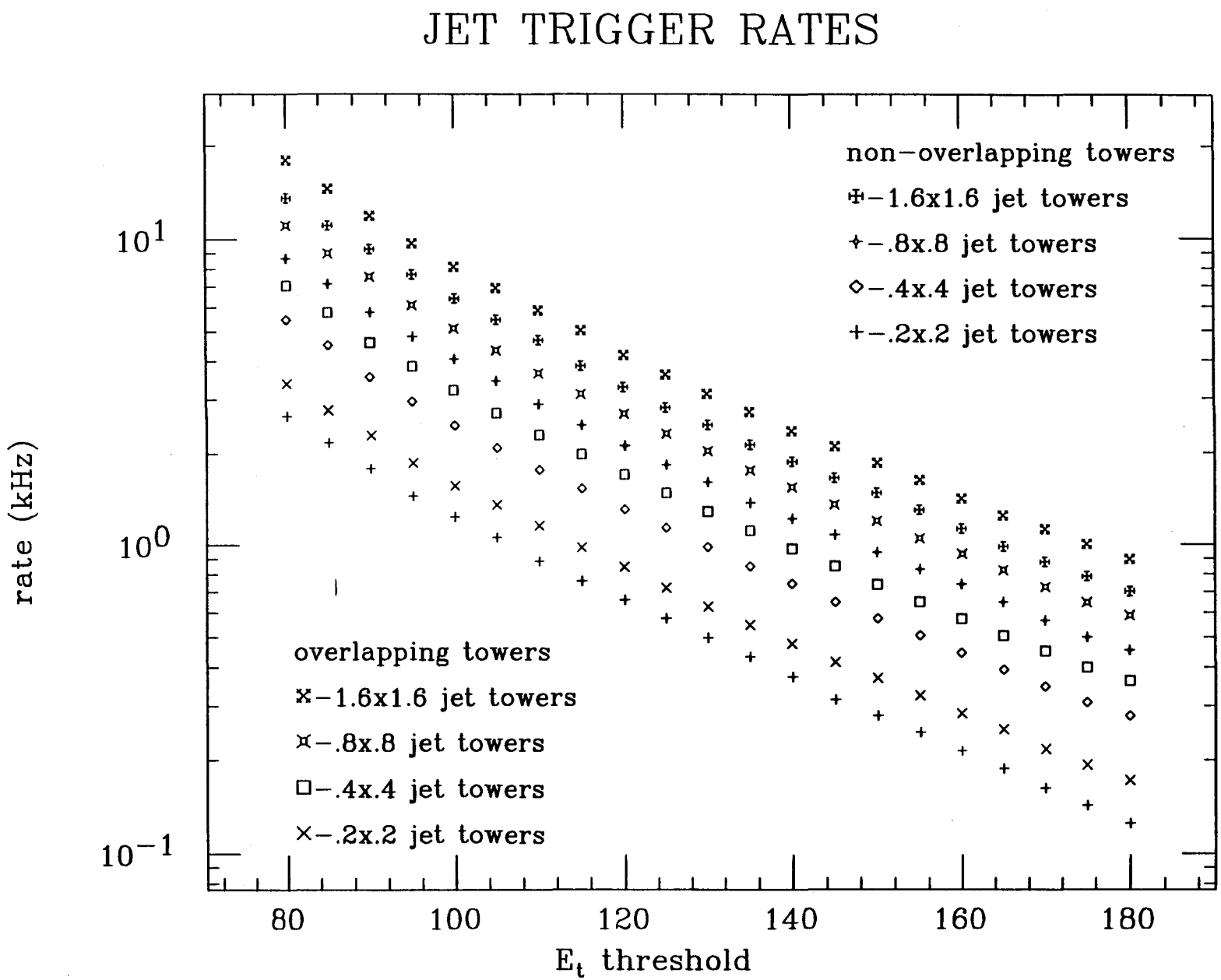
JET TRIGGER RATES
non−overlapping towers
⊞−1.6x1.6 jet towers
+−.8x.8 jet towers
◇−.4x.4 jet towers
+−.2x.2 jet towers
overlapping towers
⊠−1.6x1.6 jet towers
⌑−.8x.8 jet towers
□−.4x.4 jet towers
×−.2x.2 jet towers
rate (kHz)
10^1
10^0
10^{-1}
80
100
120
140
160
180
E_t threshold

Figure 0

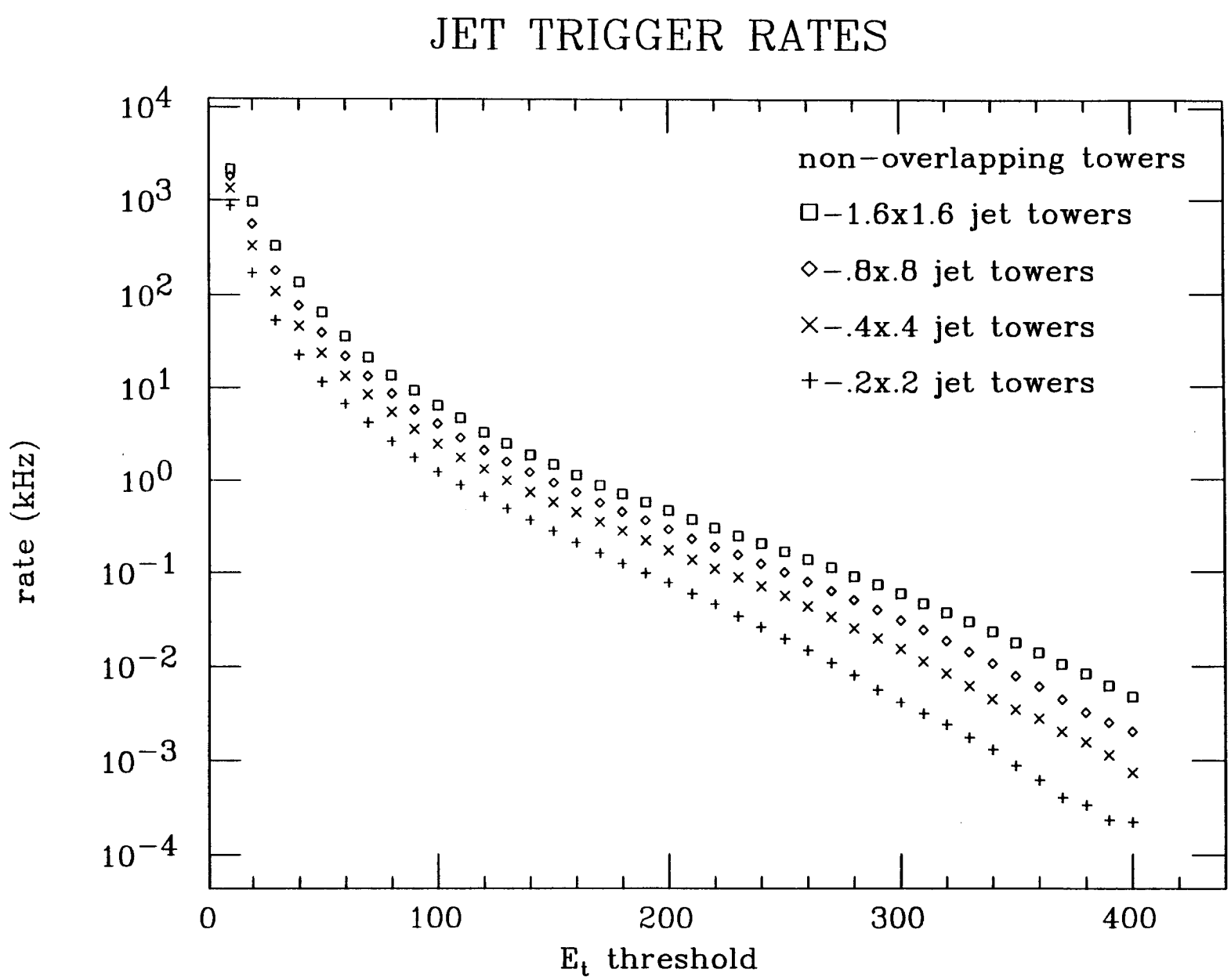
JET TRIGGER RATES
non−overlapping towers
□−1.6x1.6 jet towers
◇−.8x.8 jet towers
×−.4x.4 jet towers
+−.2x.2 jet towers
rate (kHz)
10^4
10^3
10^2
10^1
10^0
10^{-1}
10^{-2}
10^{-3}
10^{-4}
0
100
200
300
400
E_t threshold

Figure 1

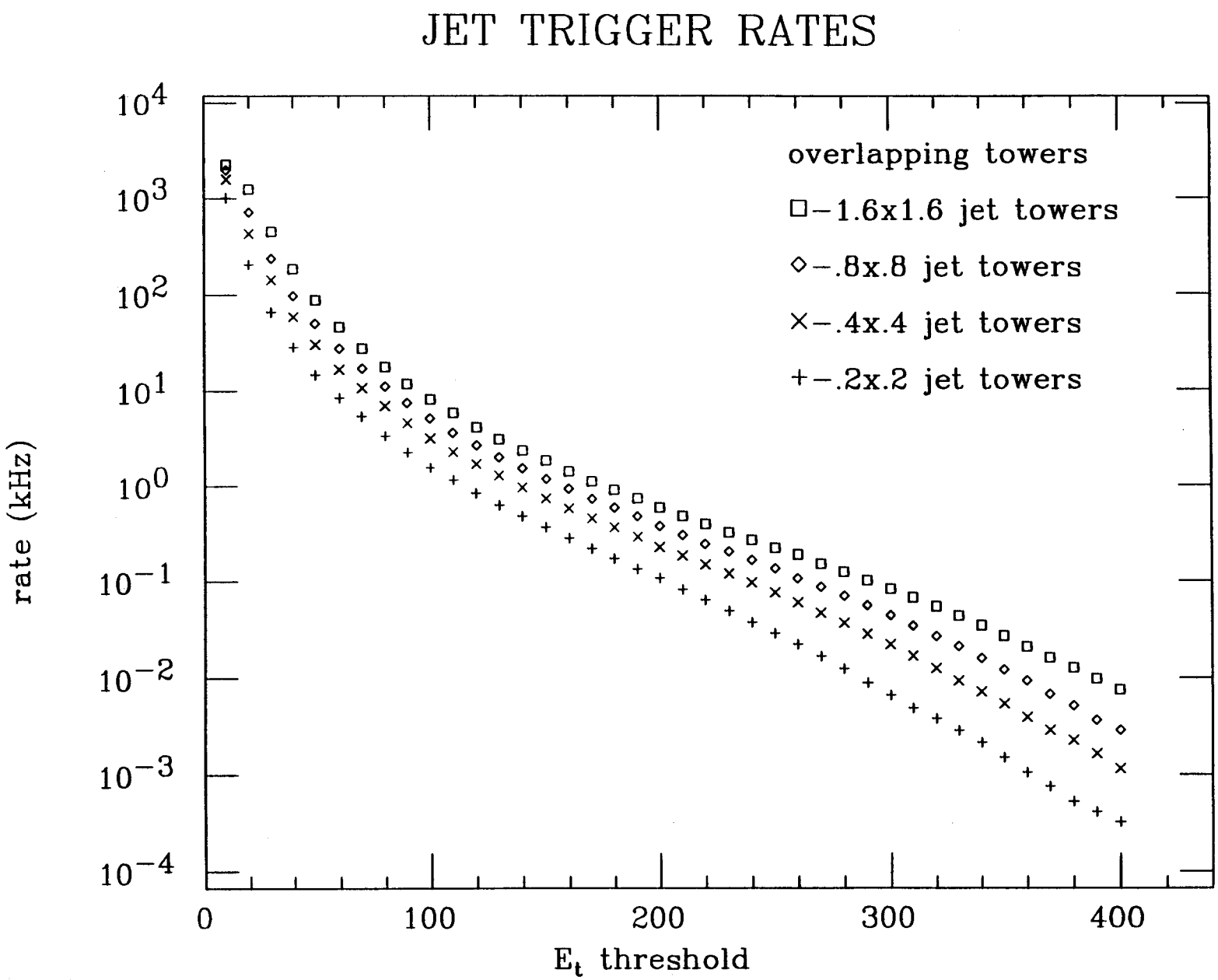
JET TRIGGER RATES
overlapping towers
□–1.6x1.6 jet towers
◇–.8x.8 jet towers
×–.4x.4 jet towers
+–.2x.2 jet towers
rate (kHz)
10^4
10^3
10^2
10^1
10^0
10^{-1}
10^{-2}
10^{-3}
10^{-4}
0
100
200
300
400
E_t threshold

Figure 2

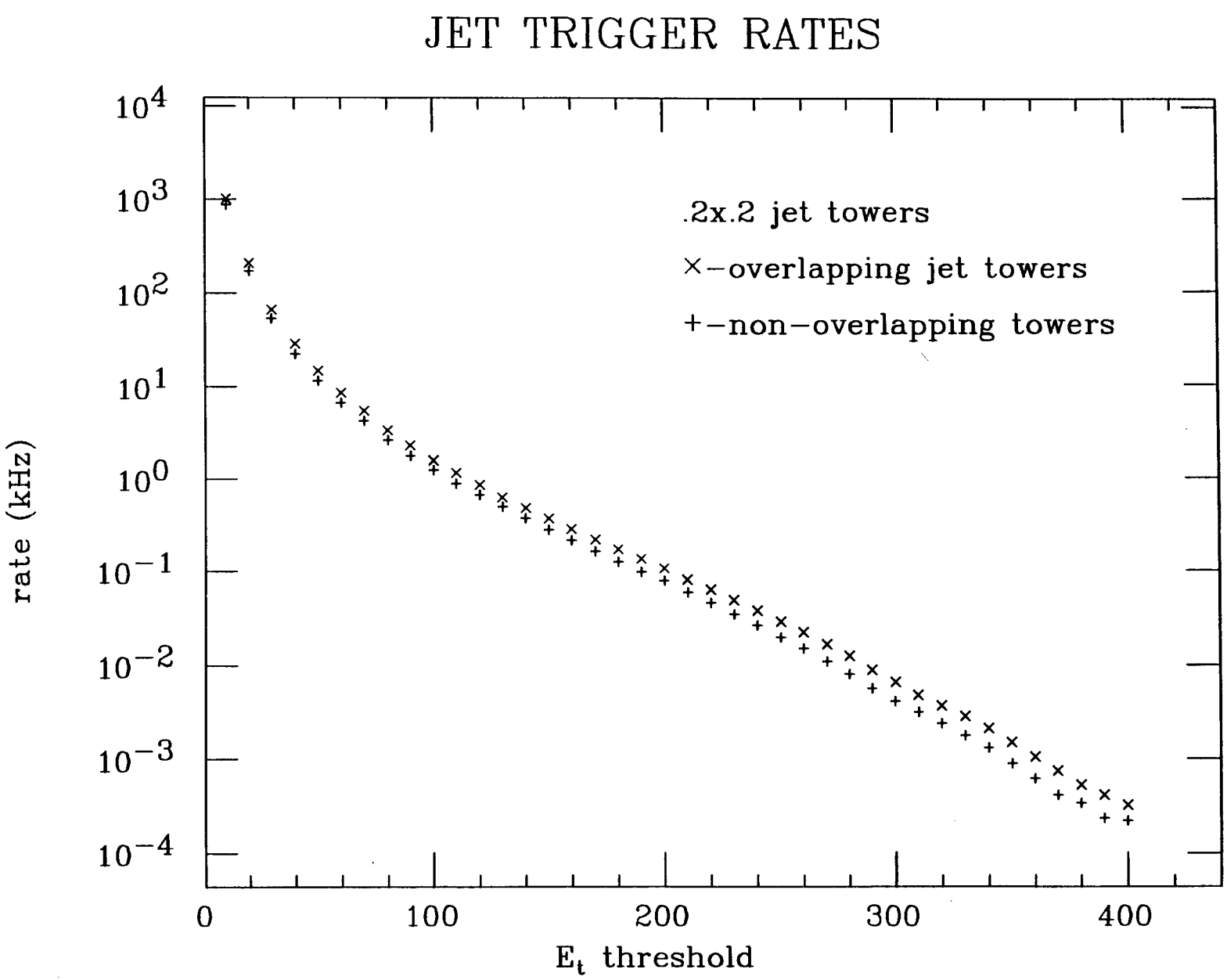
JET TRIGGER RATES
.2x.2 jet towers
×−overlapping jet towers
+−non−overlapping towers
rate (kHz)
10^4
10^3
10^2
10^1
10^0
10^{-1}
10^{-2}
10^{-3}
10^{-4}
0
100
200
300
400
E_t threshold

Figure 3

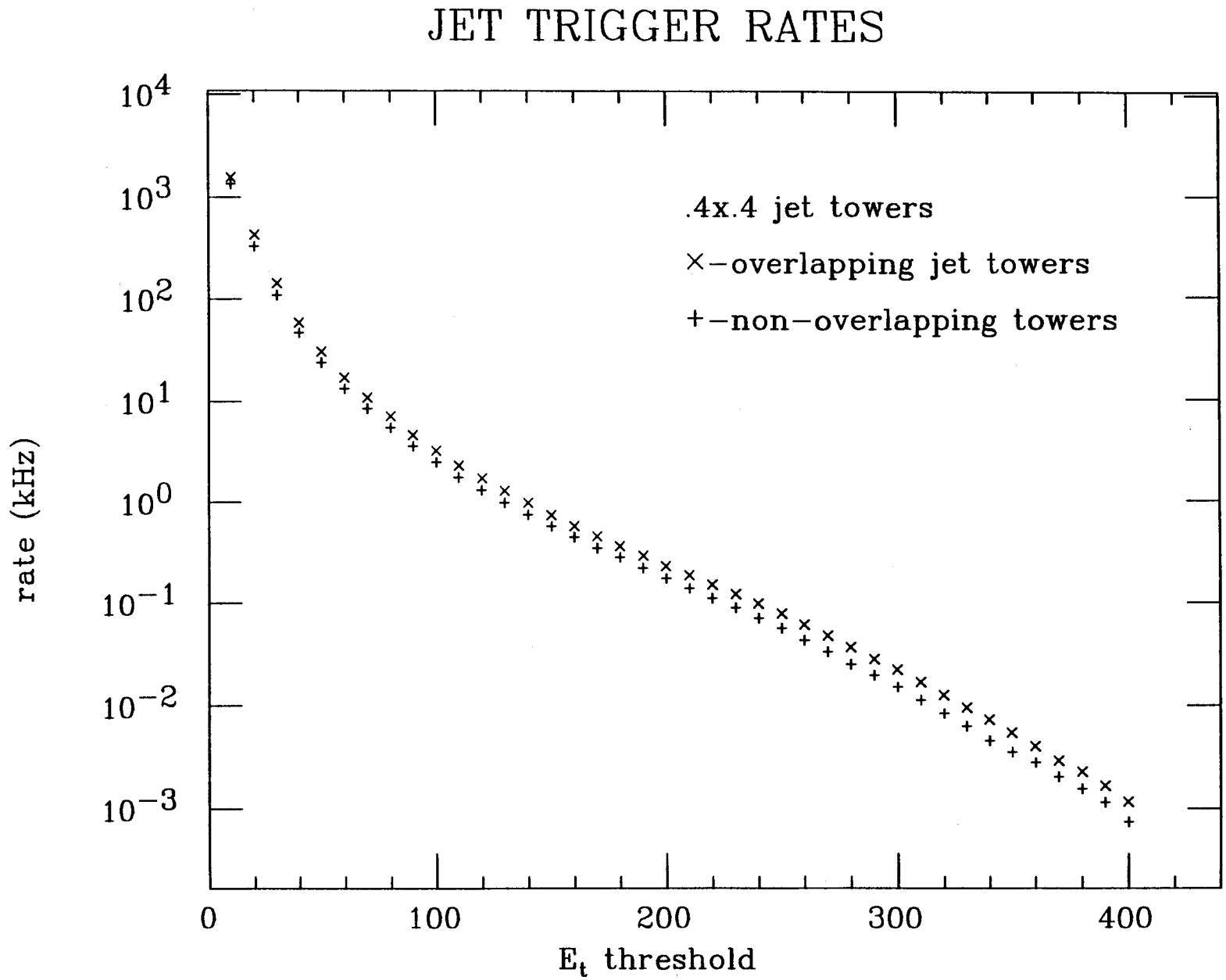
JET TRIGGER RATES
.4x.4 jet towers
×−overlapping jet towers
+−non−overlapping towers
rate (kHz)
10^4
10^3
10^2
10^1
10^0
10^{-1}
10^{-2}
10^{-3}
0
100
200
300
400
E_t threshold

Figure 4

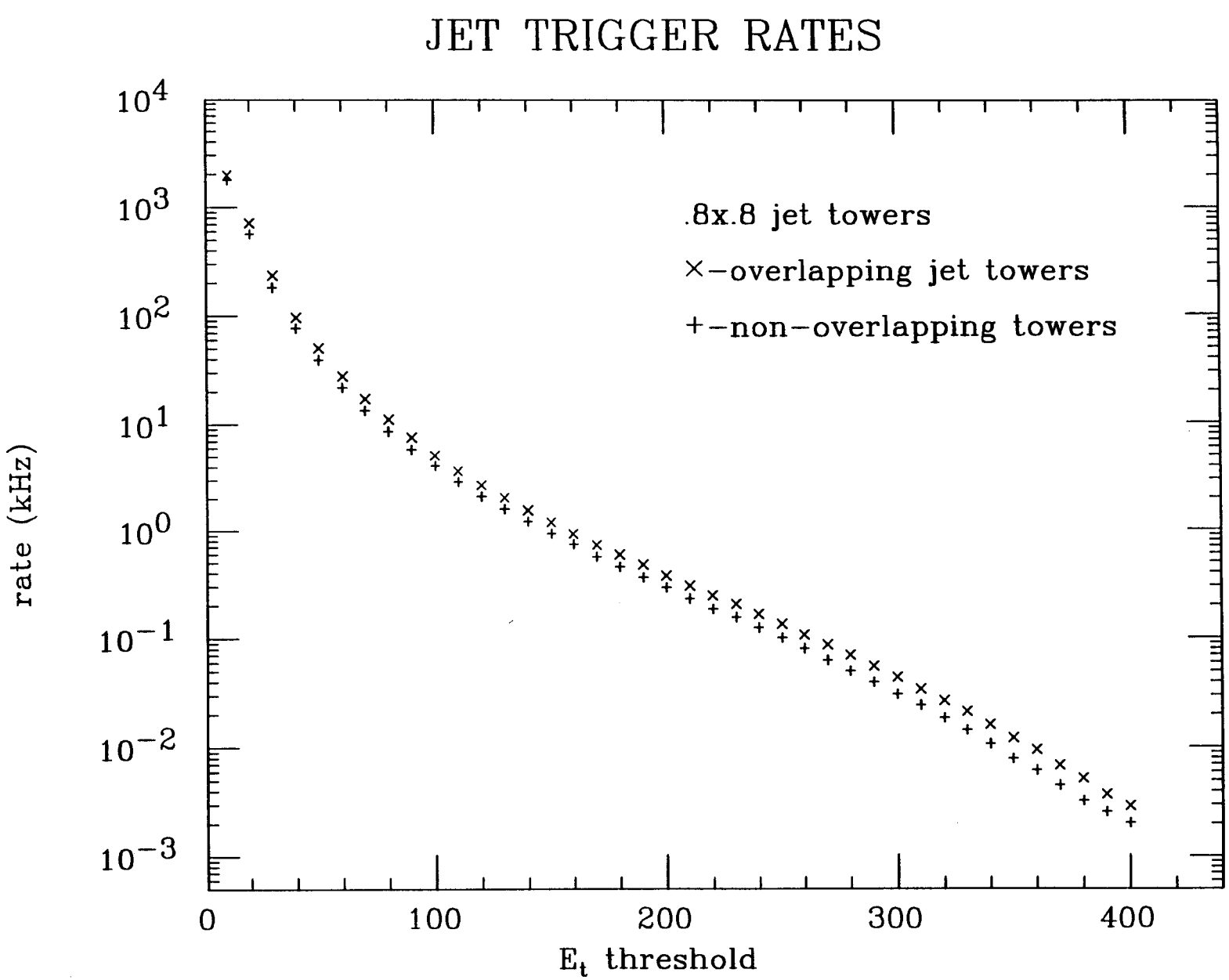
JET TRIGGER RATES
.8x.8 jet towers
×−overlapping jet towers
+−non−overlapping towers
rate (kHz)
10^4
10^3
10^2
10^1
10^0
10^{-1}
10^{-2}
10^{-3}
0
100
200
300
400
E_t threshold

Figure 5

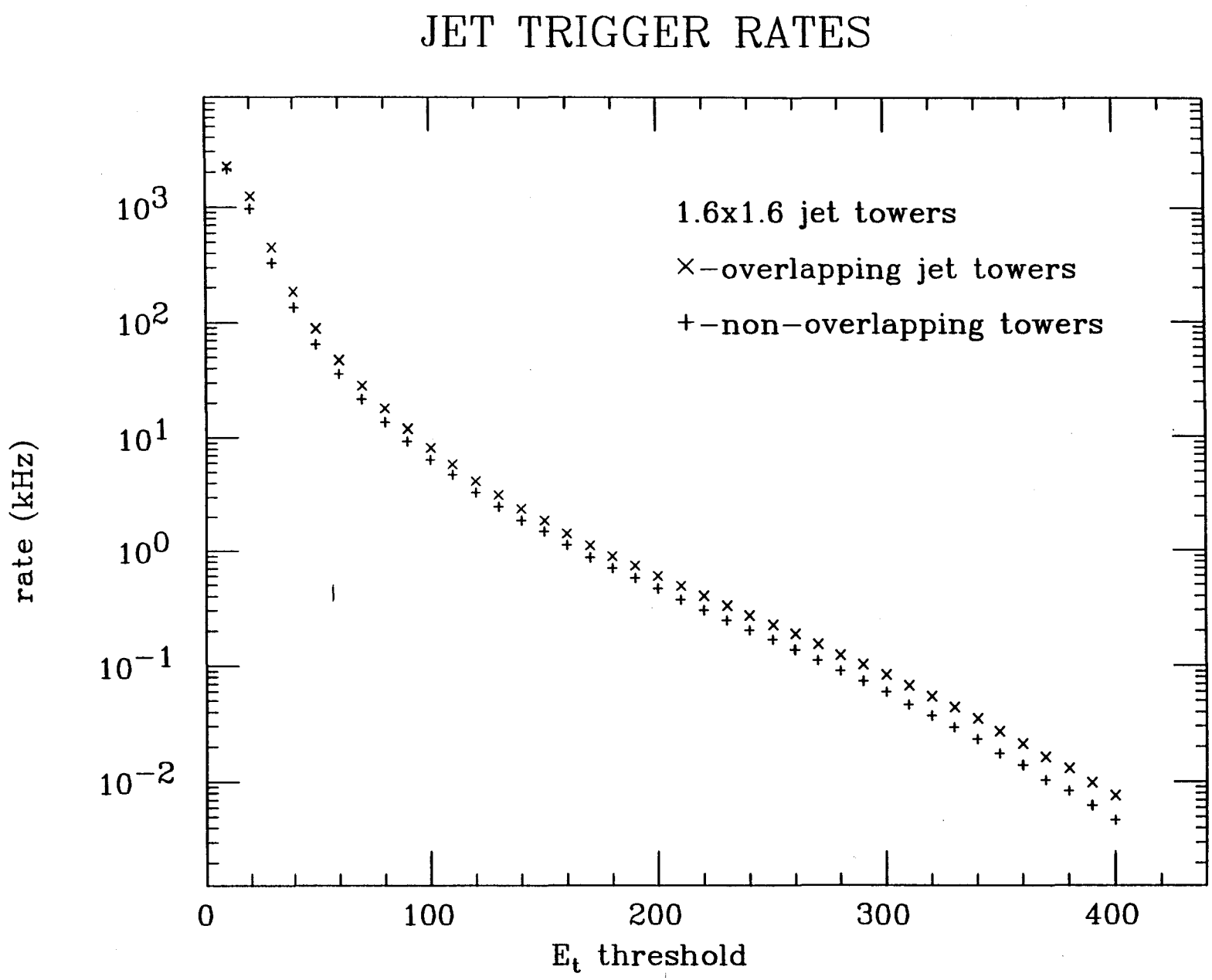
JET TRIGGER RATES
1.6x1.6 jet towers
×−overlapping jet towers
+−non−overlapping towers
rate (kHz)
10^3
10^2
10^1
10^0
10^{-1}
10^{-2}
0
100
200
300
400
E_t threshold

Figure 6

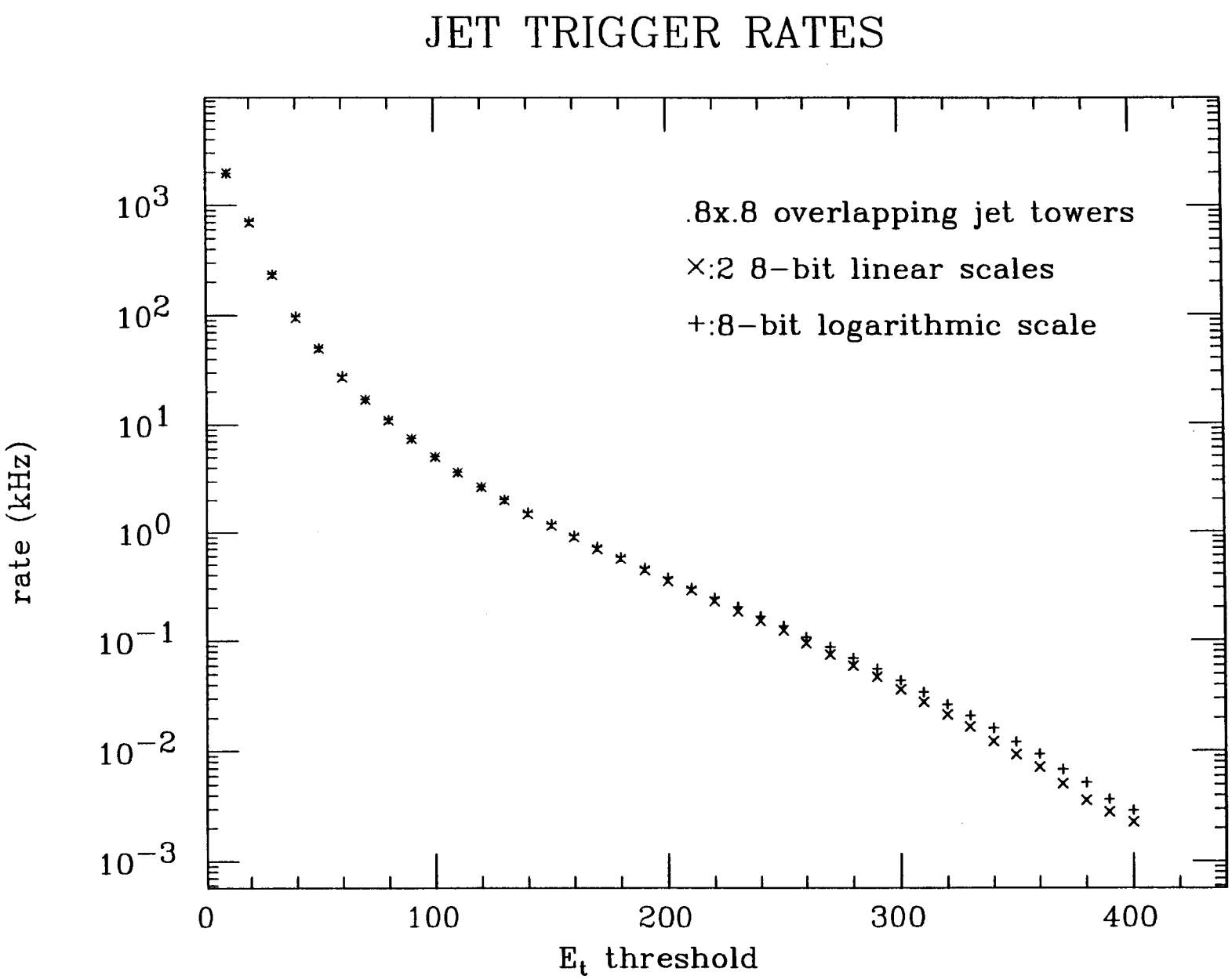
JET TRIGGER RATES
.8x.8 overlapping jet towers
×:2 8−bit linear scales
+:8−bit logarithmic scale
rate (kHz)
10^3
10^2
10^1
10^0
10^{-1}
10^{-2}
10^{-3}
0
100
200
300
400
E_t threshold

Figure 7

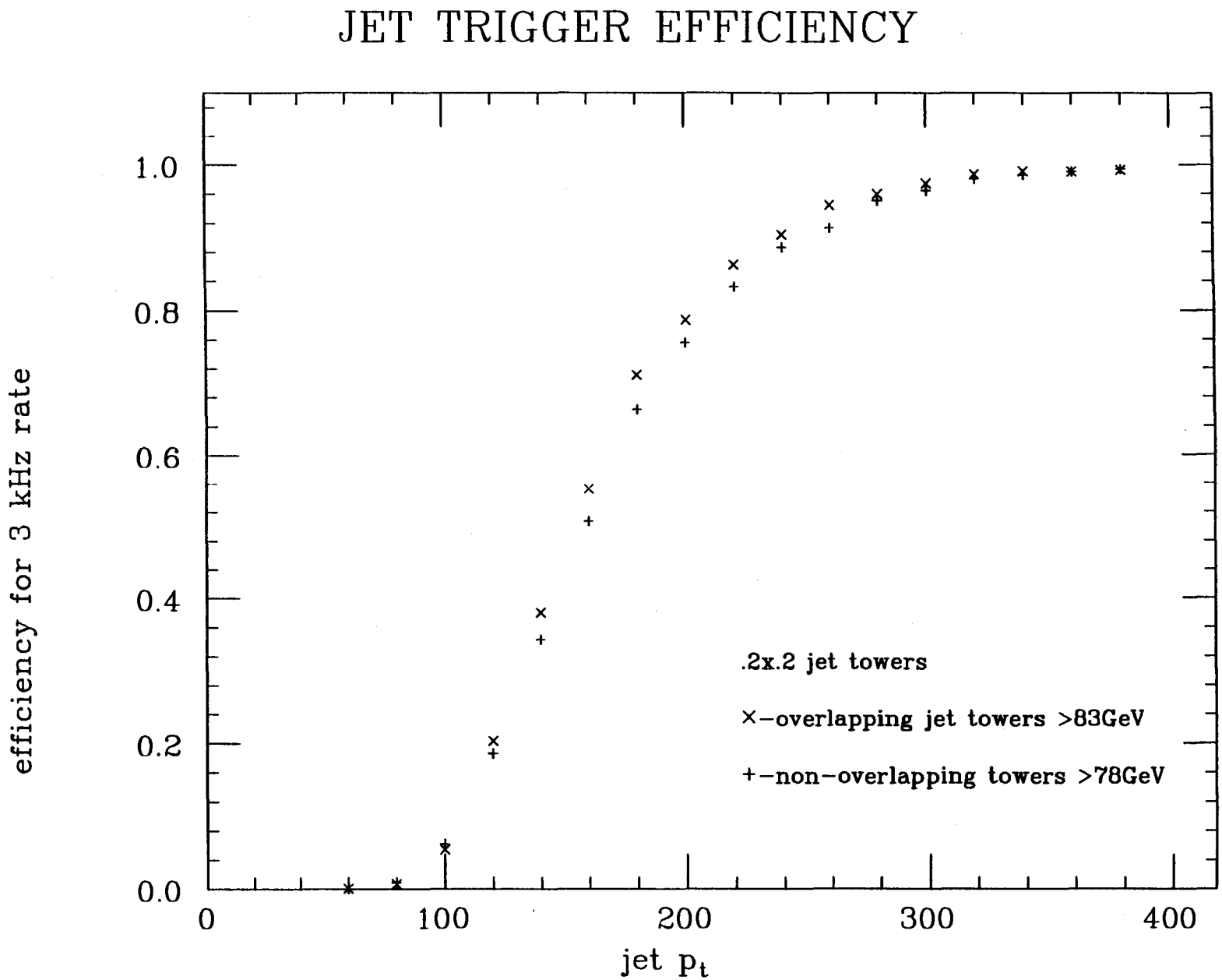
JET TRIGGER EFFICIENCY
efficiency for 3 kHz rate
1.0
0.8
0.6
0.4
0.2
0.0
0
100
200
300
400
jet p_t
.2x.2 jet towers
×−overlapping jet towers >83GeV
+−non−overlapping towers >78GeV

Figure 8

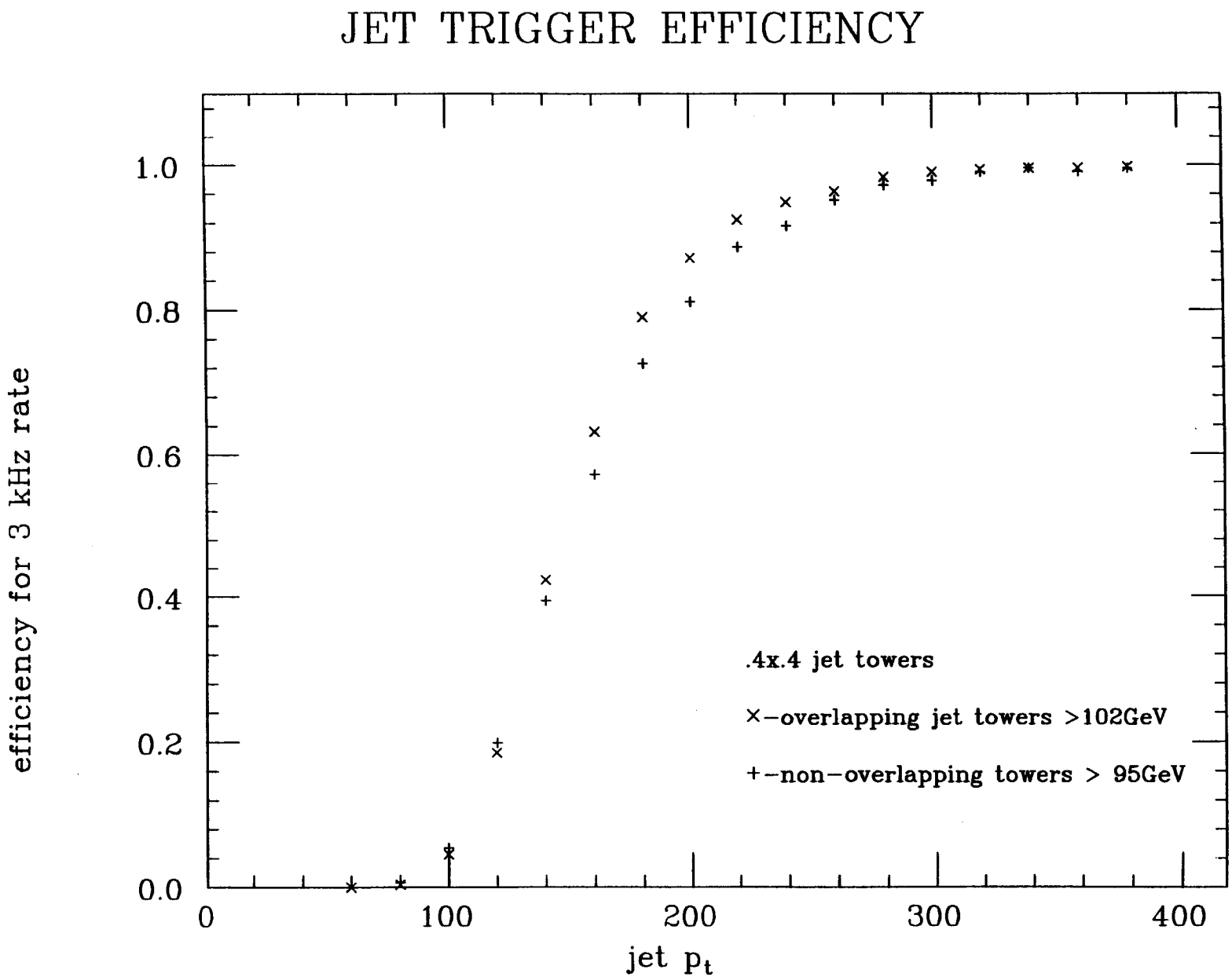
JET TRIGGER EFFICIENCY
efficiency for 3 kHz rate
1.0
0.8
0.6
0.4
0.2
0.0
0
100
200
300
400
jet p_t
.4x.4 jet towers
×–overlapping jet towers >102GeV
+–non–overlapping towers > 95GeV

Figure 9

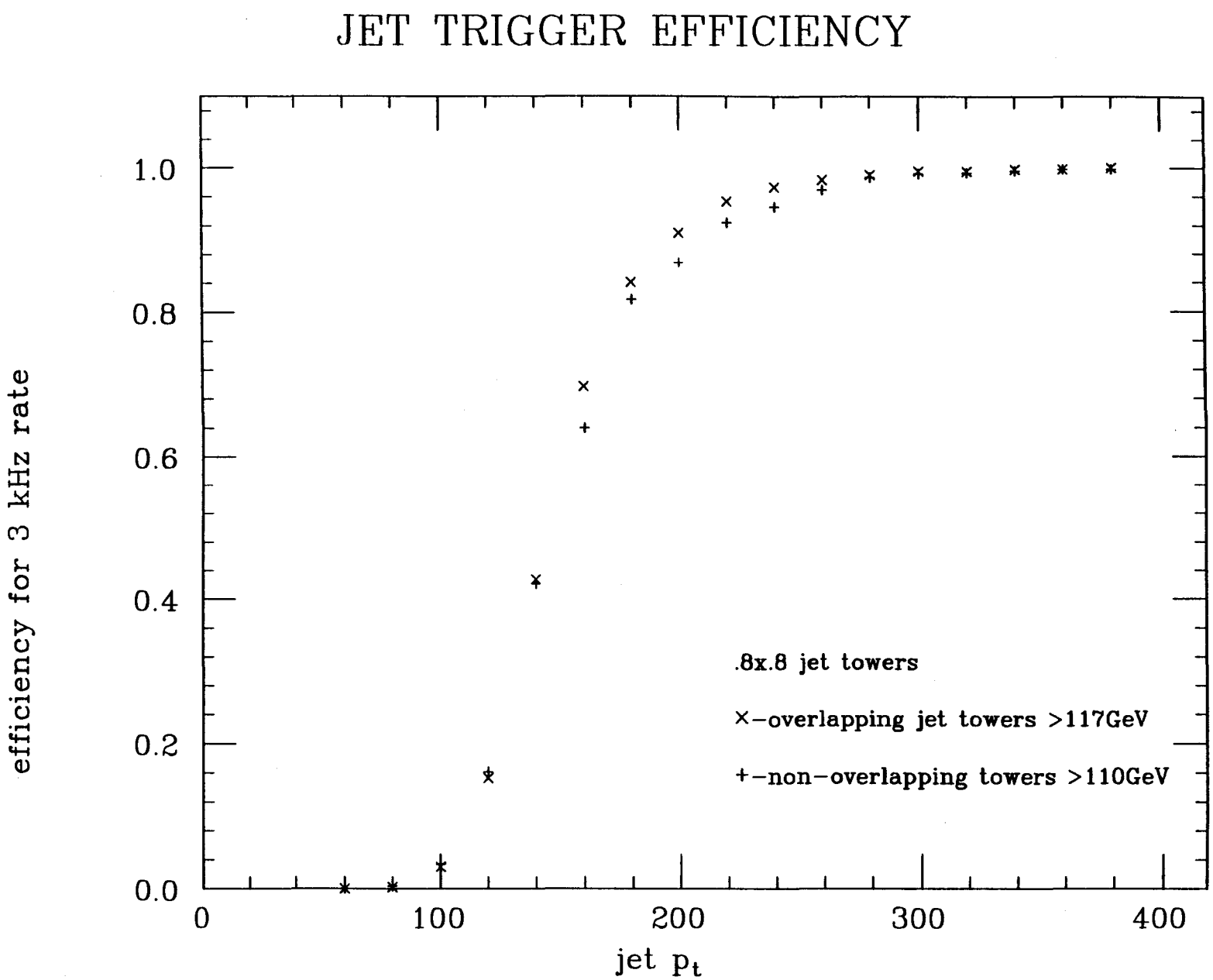
JET TRIGGER EFFICIENCY
efficiency for 3 kHz rate
1.0
0.8
0.6
0.4
0.2
0.0
0
100
200
300
400
jet p_t
.8x.8 jet towers
×–overlapping jet towers >117GeV
+–non–overlapping towers >110GeV

Figure 10

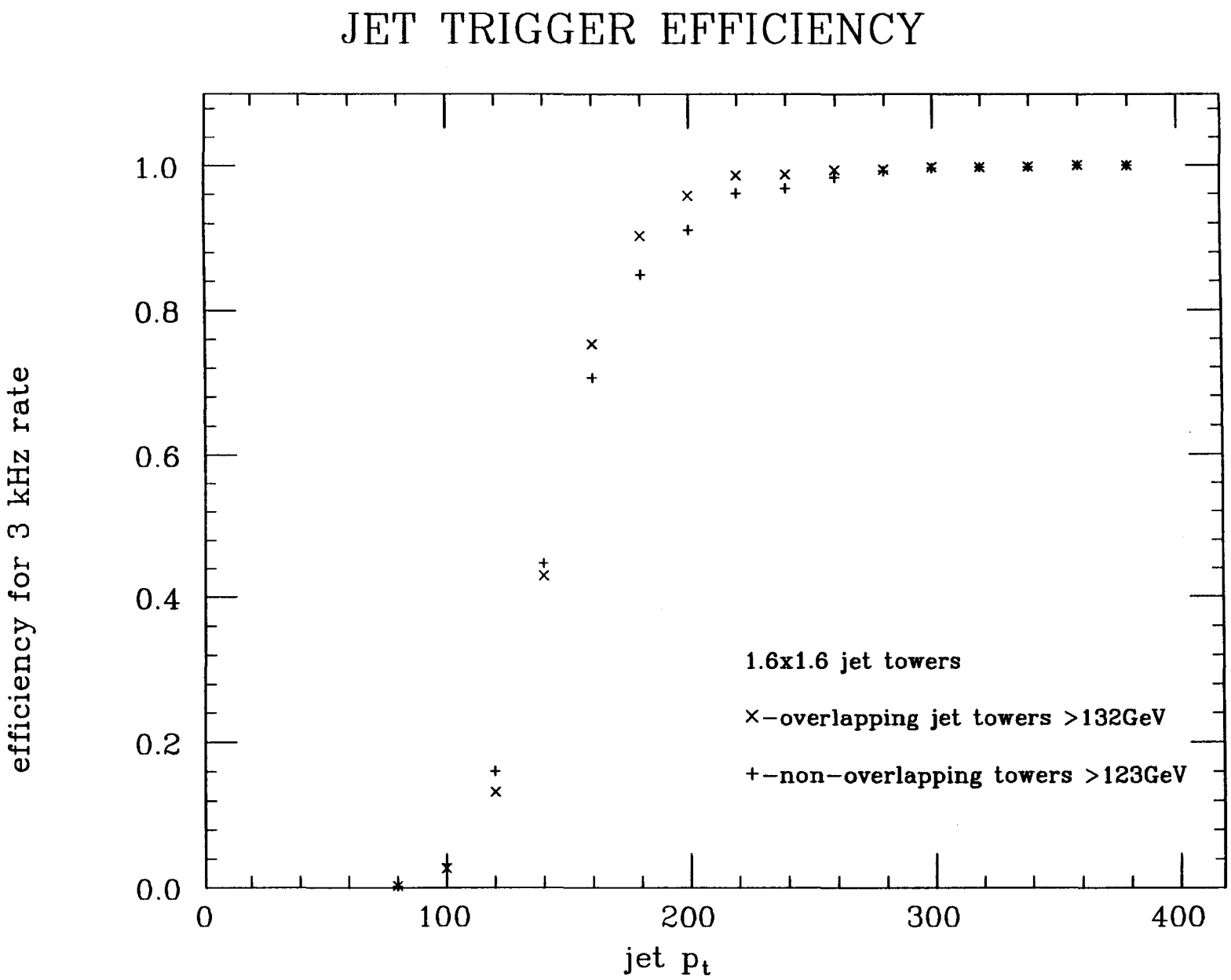
JET TRIGGER EFFICIENCY
efficiency for 3 kHz rate
1.0
0.8
0.6
0.4
0.2
0.0
0
100
200
300
400
jet p_t
1.6x1.6 jet towers
×−overlapping jet towers >132GeV
+−non−overlapping towers >123GeV

Figure 11

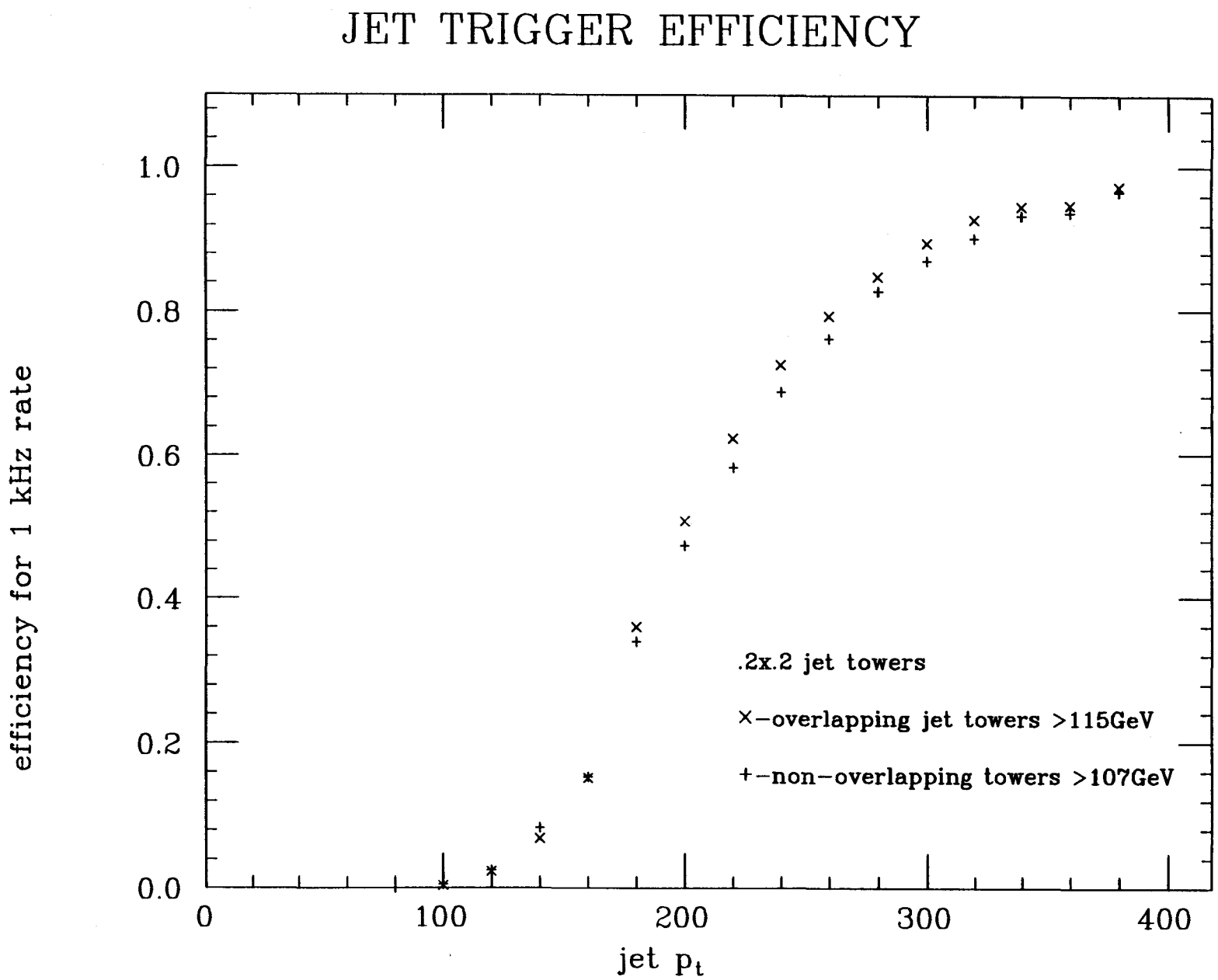
JET TRIGGER EFFICIENCY
efficiency for 1 kHz rate
1.0
0.8
0.6
0.4
0.2
0.0
0
100
200
300
400
jet p_t
.2x.2 jet towers
×−overlapping jet towers >115GeV
+−non−overlapping towers >107GeV

Figure 12

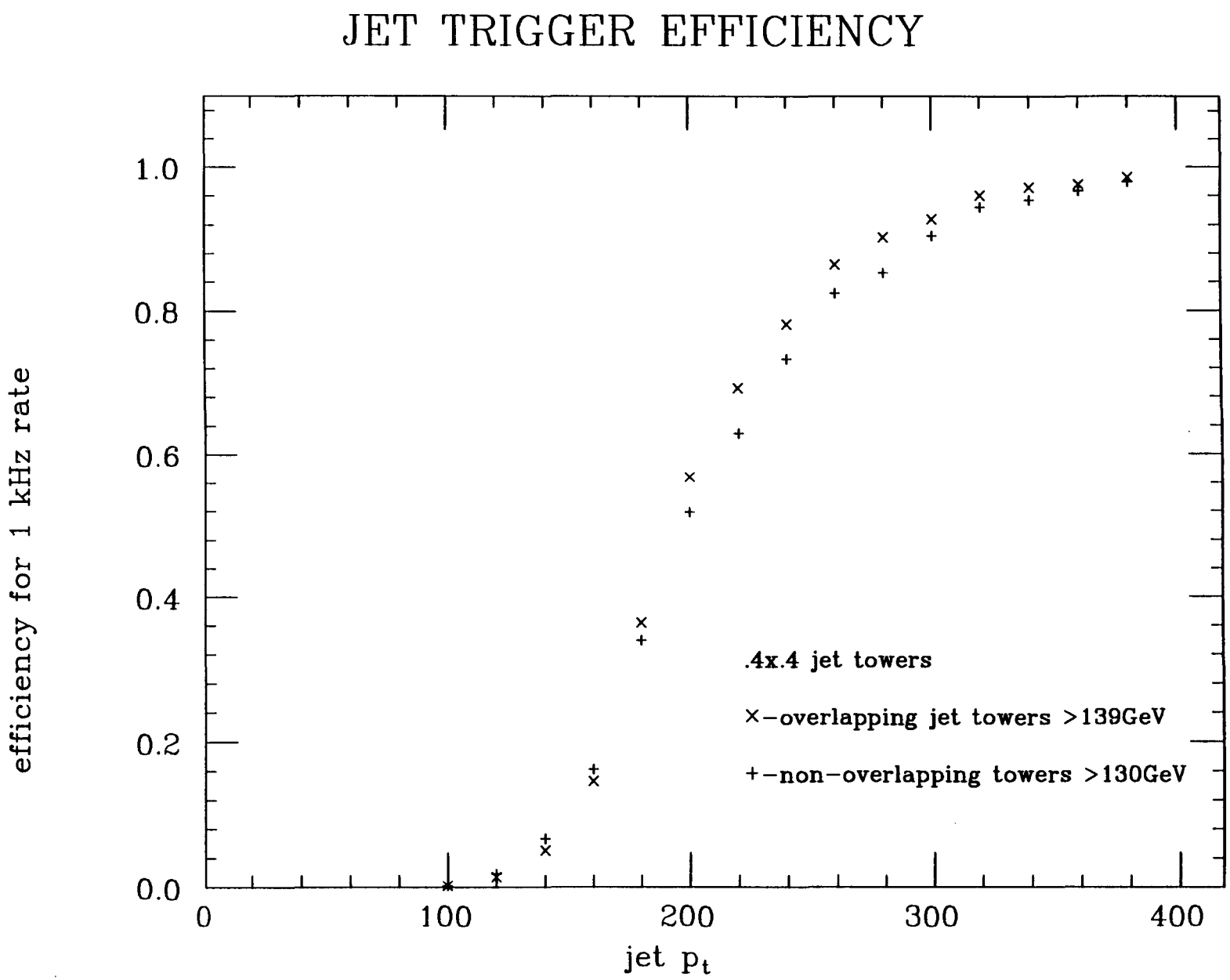
JET TRIGGER EFFICIENCY
efficiency for 1 kHz rate
1.0
0.8
0.6
0.4
0.2
0.0
0
100
200
300
400
jet p_t
.4x.4 jet towers
×−overlapping jet towers >139GeV
+−non−overlapping towers >130GeV

Figure 13

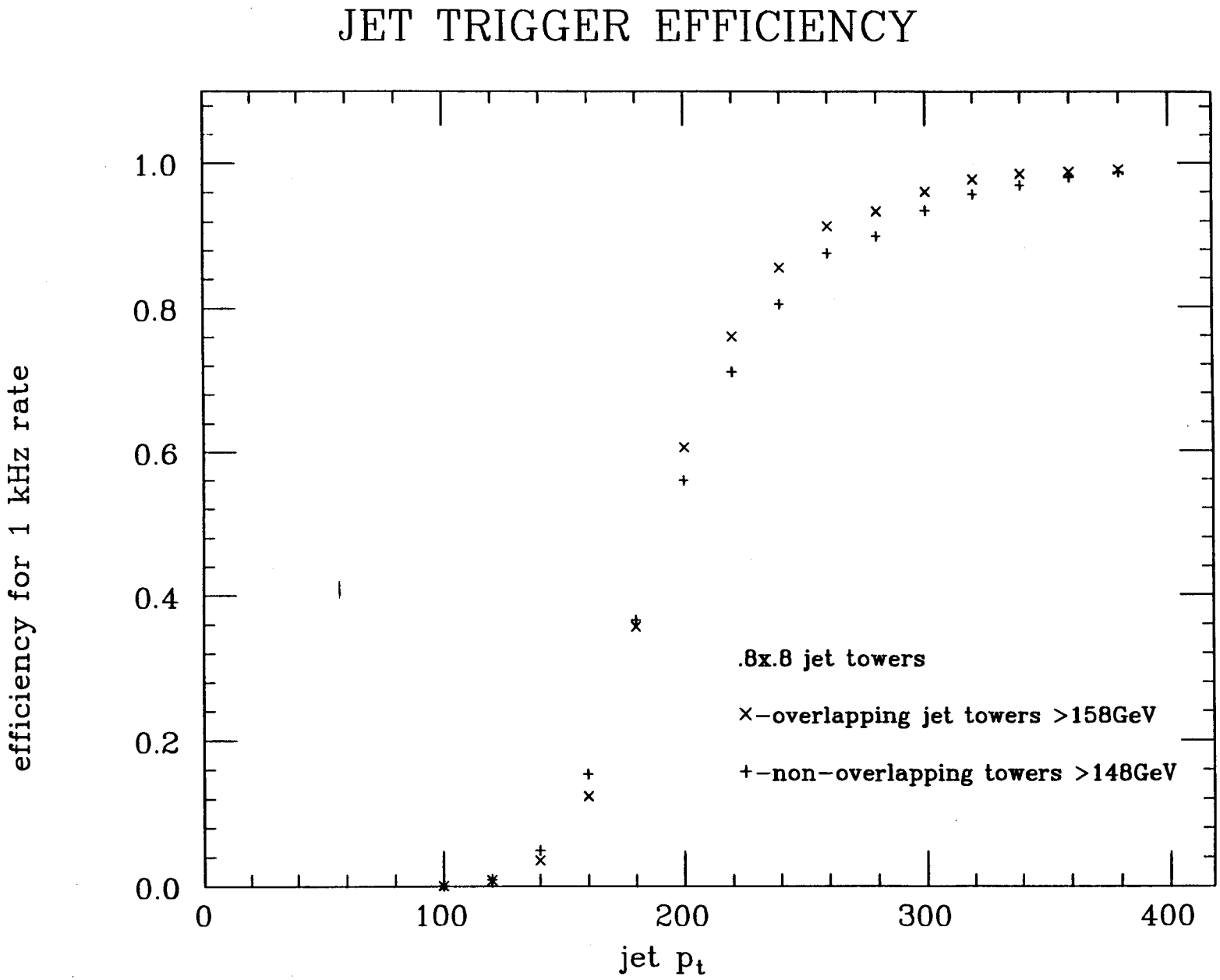
JET TRIGGER EFFICIENCY
efficiency for 1 kHz rate
1.0
0.8
0.6
0.4
0.2
0.0
0
100
200
300
400
jet p_t
.8x.8 jet towers
×–overlapping jet towers >158GeV
+–non–overlapping towers >148GeV

Figure 14

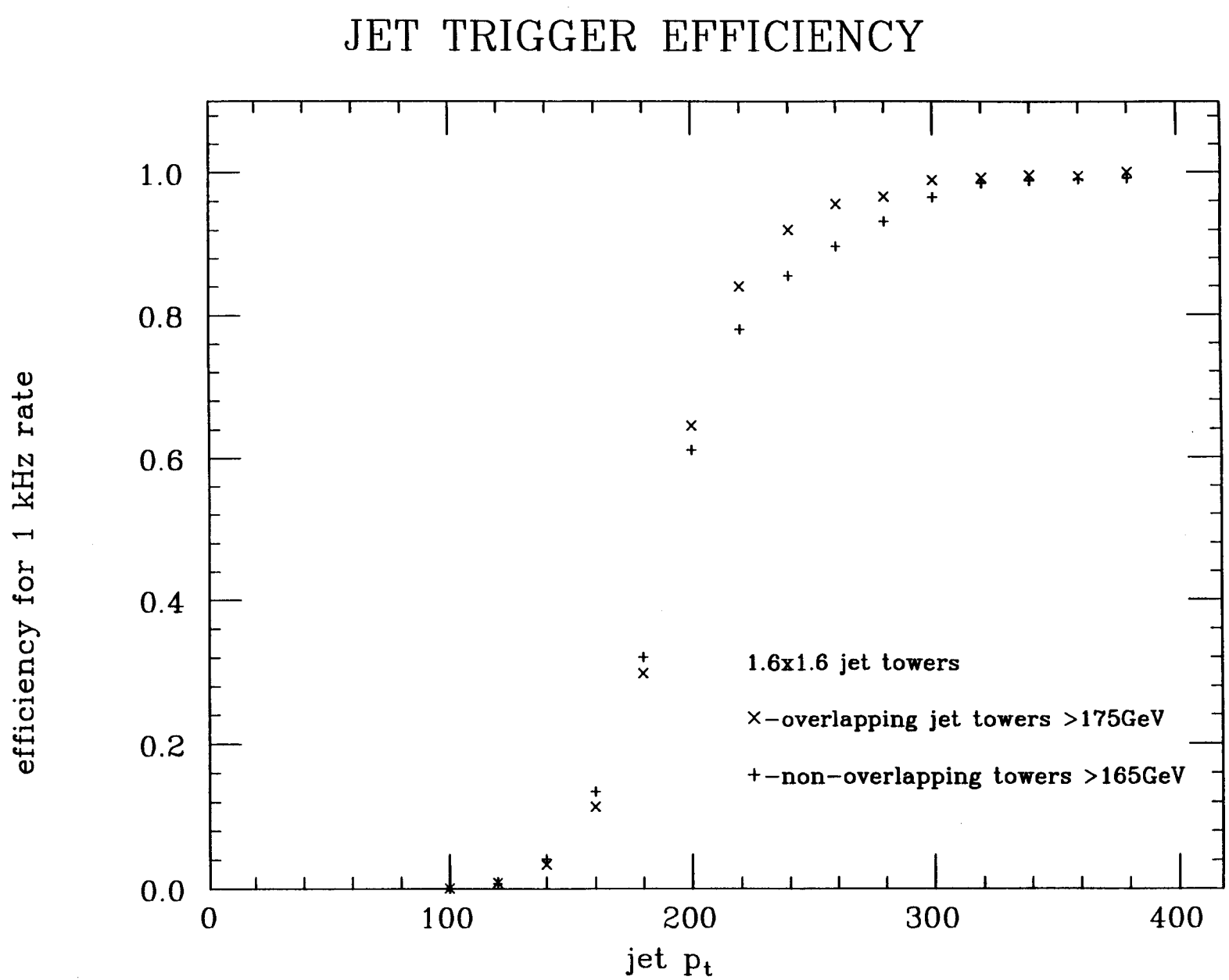
JET TRIGGER EFFICIENCY
efficiency for 1 kHz rate
1.0
0.8
0.6
0.4
0.2
0.0
0
100
200
300
400
jet p_t
1.6x1.6 jet towers
×−overlapping jet towers >175GeV
+−non−overlapping towers >165GeV

Figure 15

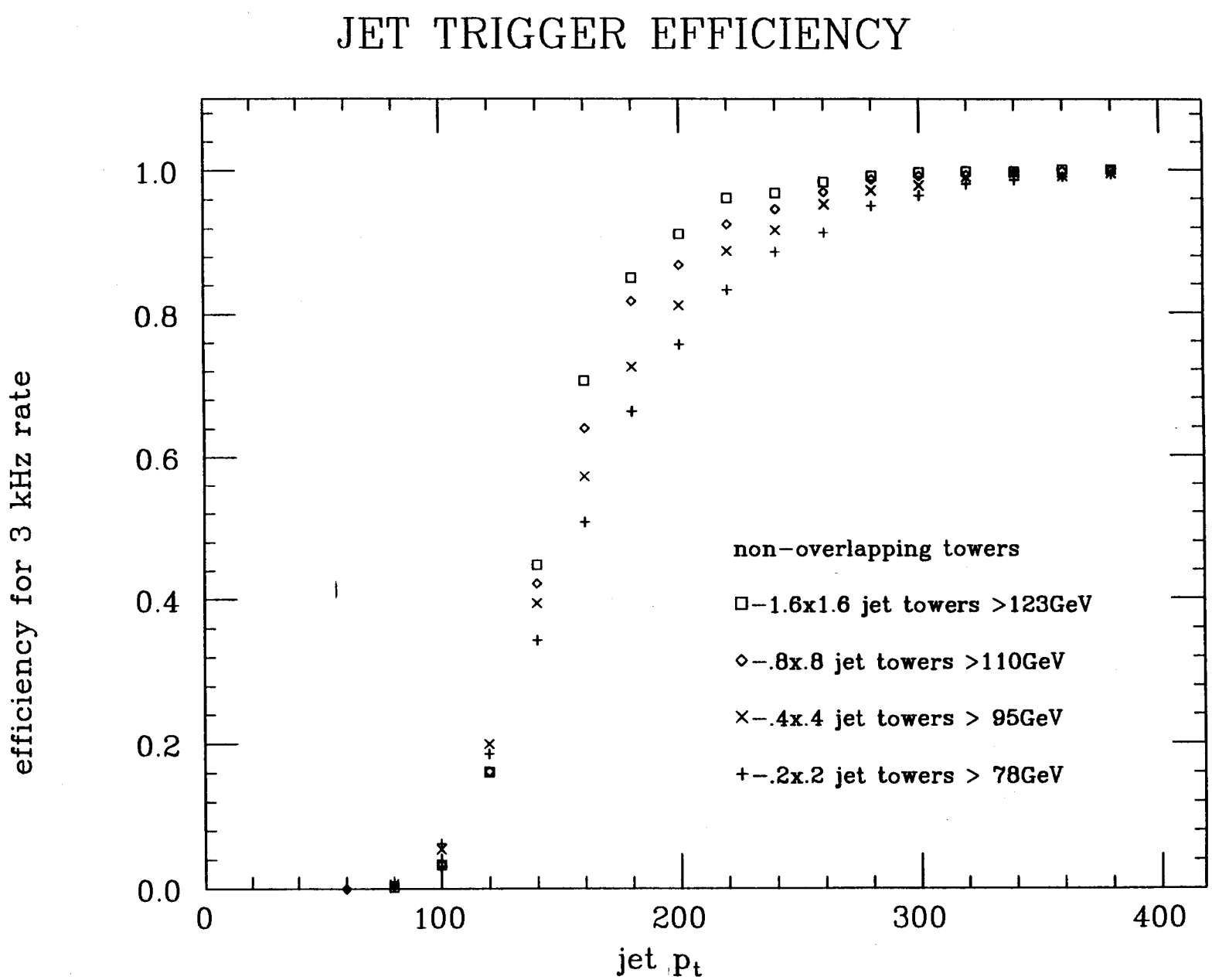
JET TRIGGER EFFICIENCY
efficiency for 3 kHz rate
1.0
0.8
0.6
0.4
0.2
0.0
0
100
200
300
400
jet p_t
non−overlapping towers
□−1.6x1.6 jet towers >123GeV
◇−.8x.8 jet towers >110GeV
×−.4x.4 jet towers > 95GeV
+−.2x.2 jet towers > 78GeV

Figure 16

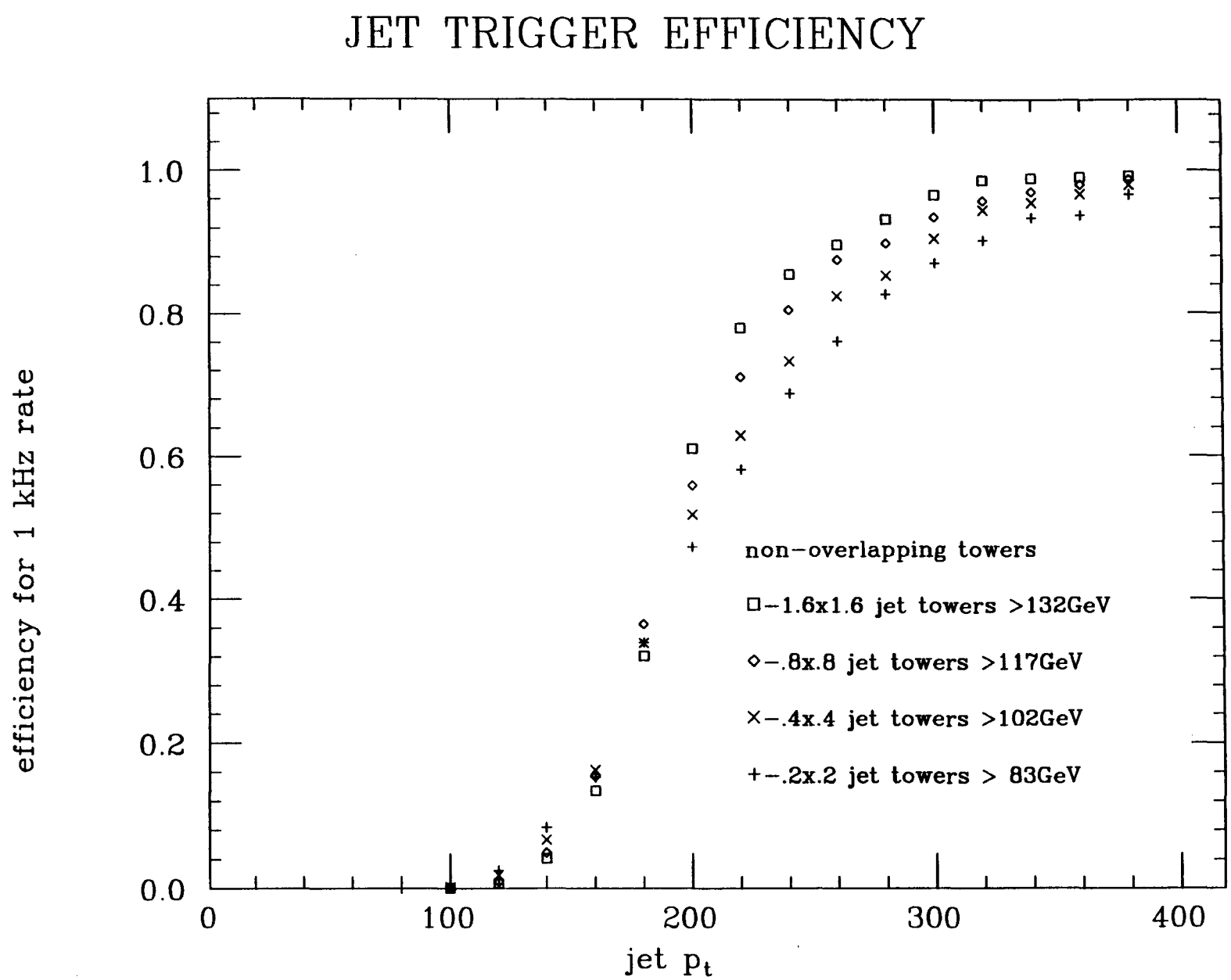
JET TRIGGER EFFICIENCY
efficiency for 1 kHz rate
1.0
0.8
0.6
0.4
0.2
0.0
0
100
200
300
400
jet p_t
non−overlapping towers
□−1.6x1.6 jet towers >132GeV
◇−.8x.8 jet towers >117GeV
×−.4x.4 jet towers >102GeV
+−.2x.2 jet towers > 83GeV

Figure 17

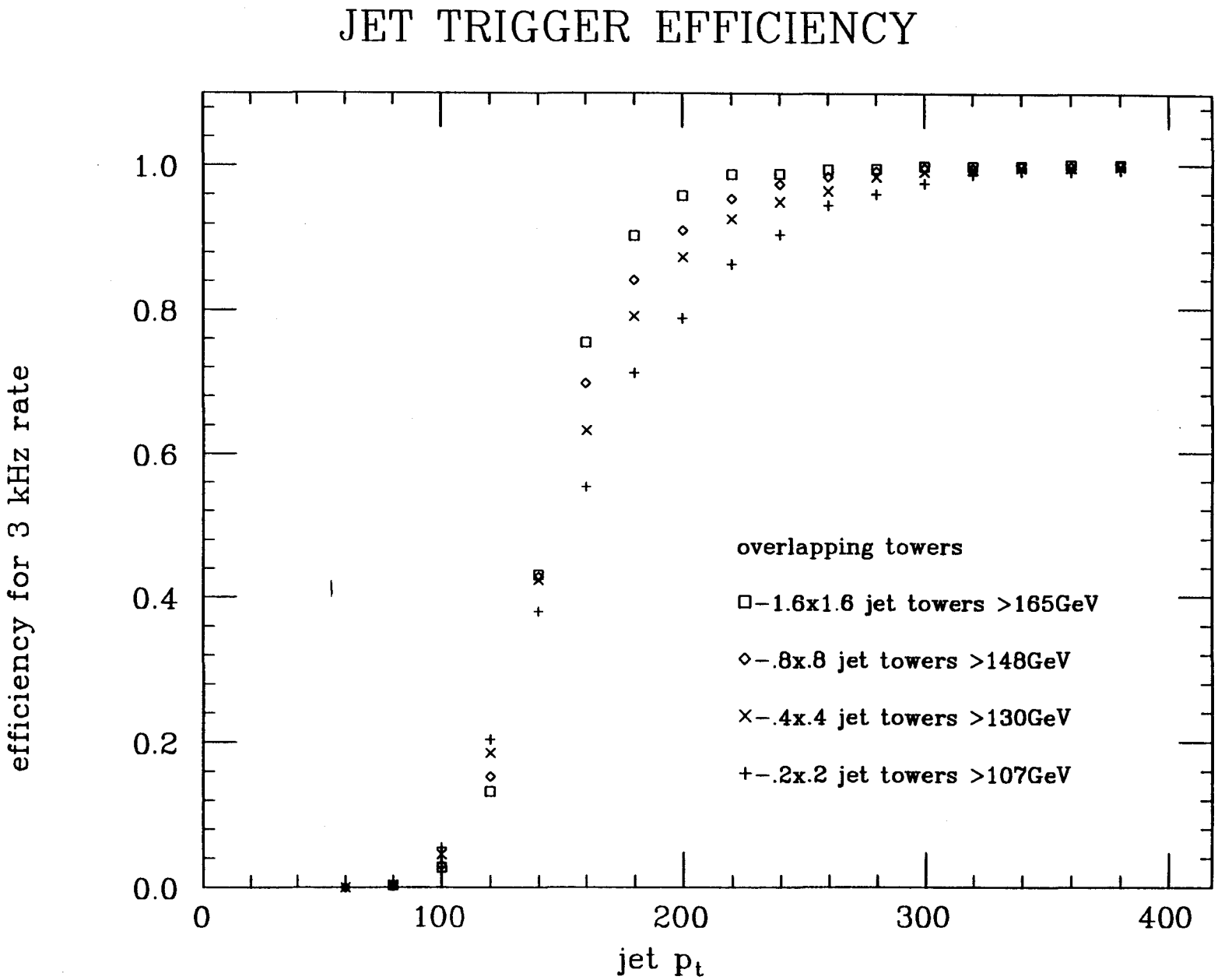
JET TRIGGER EFFICIENCY
efficiency for 3 kHz rate
1.0
0.8
0.6
0.4
0.2
0.0
0
100
200
300
400
jet p_t
overlapping towers
□–1.6x1.6 jet towers >165GeV
◇–.8x.8 jet towers >148GeV
×–.4x.4 jet towers >130GeV
+–.2x.2 jet towers >107GeV

Figure 18

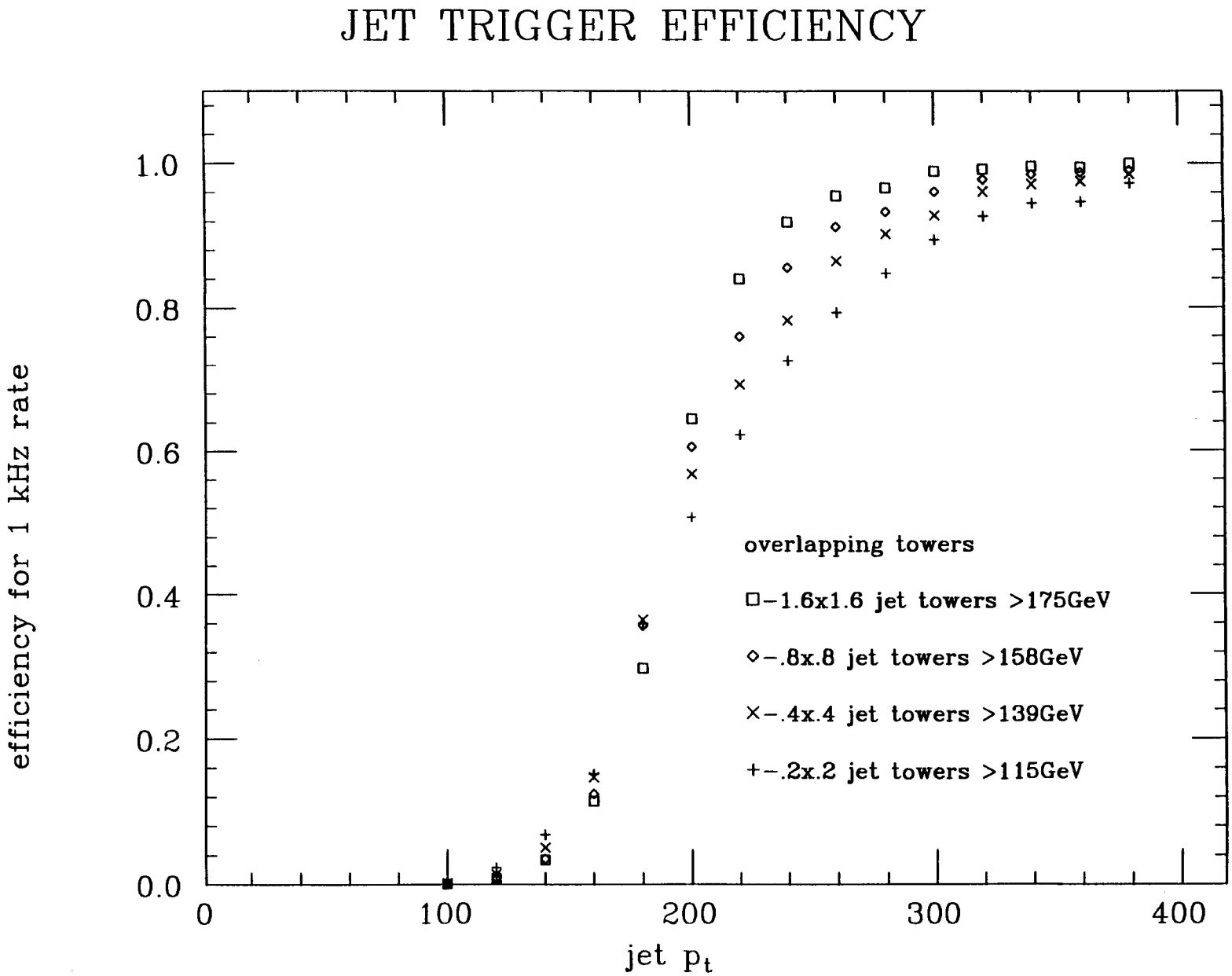
JET TRIGGER EFFICIENCY
efficiency for 1 kHz rate
1.0
0.8
0.6
0.4
0.2
0.0
0
100
200
300
400
jet p_t
overlapping towers
□–1.6x1.6 jet towers >175GeV
◇–.8x.8 jet towers >158GeV
×–.4x.4 jet towers >139GeV
+–.2x.2 jet towers >115GeV

Figure 19